

Continued development and implementation of continuous moment tensor scanning for
offshore seismicity and tsunami early warning
Final Project Report

U.S.G.S Award Number G12AP20007
Project Period January 1, 2012 to December 31, 2012

Douglas S. Dreger
University of California, Berkeley, California, 94720
Ph. (510)642-1844; Fax (510)643-5811; dreger@seismo.berkeley.edu

Abstract

In this project we have finished the implementation of Kawakatsu's (1998) GridMT method for the Mendocino region to analyze offshore earthquakes, and to develop a tsunami early warning capability for the region on an operational test bed. Through the course of this project the preliminary code has been overhauled for processing efficiency and to incorporate direct links to streaming data used by our operational system. One important modification is the development of an index-based method for eliminating the contribution of single data streams, or even entire stations, as may be necessary due to telemetry outages or other temporary station outages, without the need for rebuilding the Green's function matrices. The system is currently running in realtime and providing email notifications of event detections and moment tensor solutions.

Approach

GridMT

The GridMT method first proposed by Kawakatsu (1998) and implemented by Tsuruoka et al. (2009) recognizes that the linear moment tensor inversion is composed of the autocorrelation of Green's functions and cross correlations of Green's functions with observed waveforms. This cross-correlation may be obtained continuously on a streaming data set given adequate computational resources. Equation 1 gives the linear relationship between Green's functions (G), the moment tensor (M), and observed seismic waveforms (d).

$$GM = d \quad (1)$$

The generalized inverse solution to (1) is,

$$M = (G^T G)^{-1} G^T d \quad (2)$$

where $G^T G$ is the autocorrelation of Green's functions represented by a 6x6 matrix. This matrix and its inverse can be computed once and stored, thereby reducing processing time. $G^T d$ is the cross-correlation of Green's functions and observed waveforms, which can be computed as the data arrives. In practice we pre-compute the $(G^T G)^{-1} G^T$ matrix for an assumed velocity structure for the prescribed virtual source locations, and the locations of the stations used in the analysis. The moment tensor is then simply the cross-correlation of this inverse matrix with streaming data, and can be performed in realtime.

Tsuruoka et al. (2009) show that their GridMT method can process 7000 virtual point-sources, representing a 2.4 degree x 2.4 degree x 90 km (depth) grid sampled by a 0.1 degree laterally and 9 km in depth, in realtime on a Intel Xeon 3.06 GHz machine. They process 120 seconds of waveform data every 2 seconds monitoring a variance reduction (VR) goodness of fit parameter. When the fitting parameter exceeds a threshold ($VR \geq 65\%$) an event is declared. The grid node with the best VR gives the location of the event, and the moment tensor and origin time of the event are determined simultaneously.

Results

Testing Capability for the March 11, 2011 Tohoku-oki Mw9.0 earthquake

In our previous NEHRP (G10AP00069) project we developed the quasi-finite-source Green's function (QFSGF) extension to GridMT (Guilhem and Dreger, 2011). We have tested the modified method using strong motion data recorded for the March 11, 2011 Mw 9.0 Tohoku-oki earthquake, and have published a paper (Guilhem et al., 2012; included in appendices) on the performance. The results of this analysis reveal that the modified method is indeed capable of autonomously detecting, locating and determining an unsaturated moment tensor solution for the Mw 9.0 earthquake within a 8 minute time frame using very long period acceleration recordings. This time frame is controlled by 1) wave propagation delays across the network for the very long-period (100 to 200 seconds) data that is used; and 2) the time required for stabilization of the recursive filters that are applied to streaming data. Thus the method would be capable of maintaining pace with streaming data approximately 8 minutes behind realtime, potentially enabling a 20+ minute warning for damaging tsunami waves.

Implementation of GridMT in Mendocino

This project focused on software refinements to establish an operational test bed to evaluate performance. Following this test and analysis the plan is to migrate the processing into the operational Berkeley Seismological Laboratory (BSL) monitoring system in the future.

The following major refinements were made.

First, we have eliminated the need for instrument correction of the streaming data by convolving the Green's function database with the appropriate response functions for the four employed stations (HOPS, ORV, WDC and YBH). Thus processing is now performed on raw streaming velocity component data from these stations by applying a recursive bandpass Butterworth filter with corners between 0.02 to 0.05 Hz. The current system inverts 380 seconds of data from 12 channels every 2 seconds for 5000 virtual sources distributed over the Mendocino region. Goodness of fit, variance reduction, is used to provide event detection (variance reduction exceeding 60%). The virtual source with the greatest fit provides the location of the earthquake. The processing thus obtains location, origin time, moment magnitude and source mechanism from an independent detection of earthquake occurrence.

Second, the software was interfaced with waveform server software developed for the earthquake early warning system at the BSL. This modification allows direct access to waveform data from the operational system buffers.

Third, since this system is always running on streaming data changes to the station configuration due to failed telemetry links or mechanical failure of a station or component of a station has a substantial negative impact on performance. Our old code required rebuilding G and $(G^T G)^{-1} G^T$ matrices each time the station configuration changes. In the new code we have established an approach eliminating contributions from offending channels or stations by adjusting the indexing in the matrix operations. When channels and stations are returned to service it is now a straightforward adjustment to the code allowing a rapid restart avoiding the time consuming process of generating the Green's function databases.

Figure 1 shows the location of virtual sources (gray plusses) and results from Guilhem et al. (2011). The virtual sources extend from a depth of 5 km to 38 km with 3 km intervals. Since

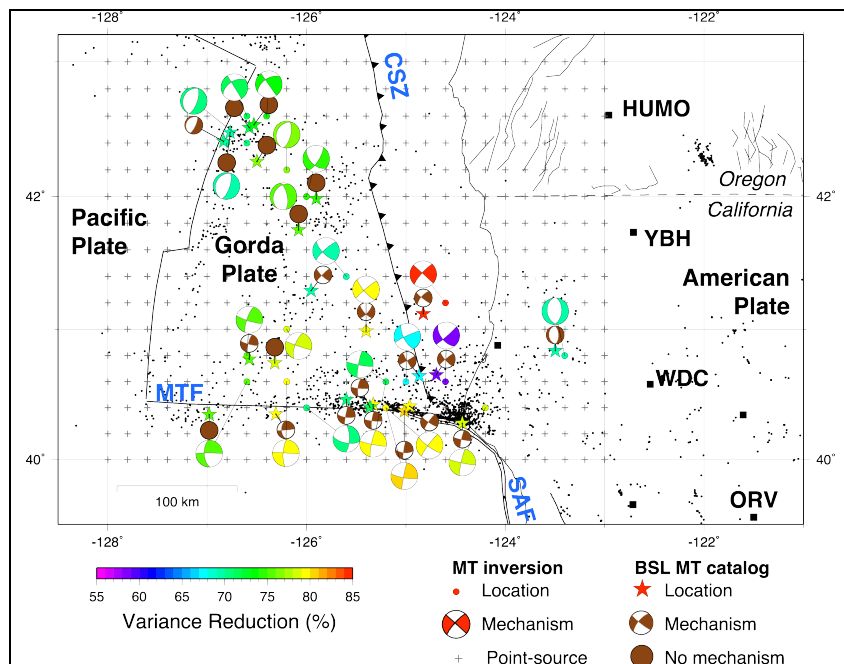


Figure 1. Map showing the location of Mendocino and Northern California seismicity (small black dots), source grid nodes (gray plusses), the four BDSN stations used in the analysis, and a comparison of GridMT moment tensors (color coded for level of fit) and catalog moment tensor solutions (brown). From Guilhem and Dreger, 2011.

October 31, 2012 the refined version of GridMT has been running on the test bed system. We reported on the initial performance at the April 19, 2013 Seismological Society of America Meeting (Guilhem et al., 2013). At that time there were 19 detections of events with a variance reduction exceeding 60%, and two offshore M4 earthquakes were missed. These events were missed because of elevated noise levels resulting in a goodness of fit less than the 60% threshold.

Of the 19 detections 5 were found to be due to a noise spike on the east component of the YBH station. These false detections have been eliminated by removing this component from processing while repairs are being made to the mechanically failing instrument. The code producing false detections in this case can be considered a benefit since the continuous analysis of the low-frequency wavefield allowed the rapid identification of a failing component of the network.

Three of the detections were due to teleseismic surface waves. Such detections are problematic, however the rate is much lower than the rate of similarly sized teleseismic events that occur every few days globally and are therefore the teleseismic event detections are fairly rare. These detections are characterized by locations at the edges of the processing grid, which raises suspicion. We anticipate that the addition of a northern station as described below will likely reduce the rate of teleseismic event detection.

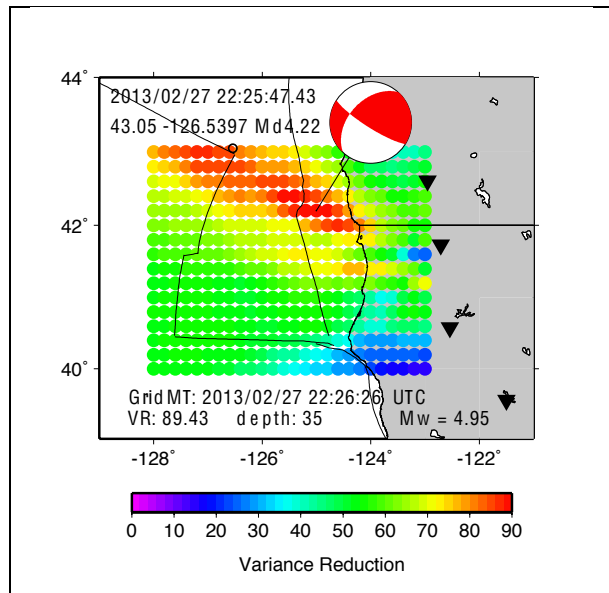


Figure 2. Map showing goodness of fit for a 02/27/2013 Mw4.9 Blanco Fracture Zone event. The actual location is shown as the black circle.

The remaining 11 events were true regional event detections located within the Gorda plate, along the Mendocino fault, and the Blanco Fracture Zone. The Blanco Fracture Zone events are located outside of the processing grid. Figure 2 shows the location performance for one of the events. To avoid these mislocations we are expanding the grid to include the Blanco Fracture Zone, and we are discussing with the University of Washington adding one of their broadband stations further north to provide additional constraint on event locations. Figure 3A shows an apparent saturation of GridMT Mw, however analysis revealed that this is due to poor magnitudes in the catalog for events located far offshore. In each case the GridMT Mw was found to be robust. Figure 3B shows mislocation for events with goodness of fit greater than (red) and less than 60% (blue). The four cases with mislocation larger

than 150 km are Blanco fracture zone events. The case with a mislocation of 140 km was for a Mw5 offshore event when data from only two of the four stations was available. The median mislocation for the remaining events is approximately 50 km, which is essentially two virtual source nodes.

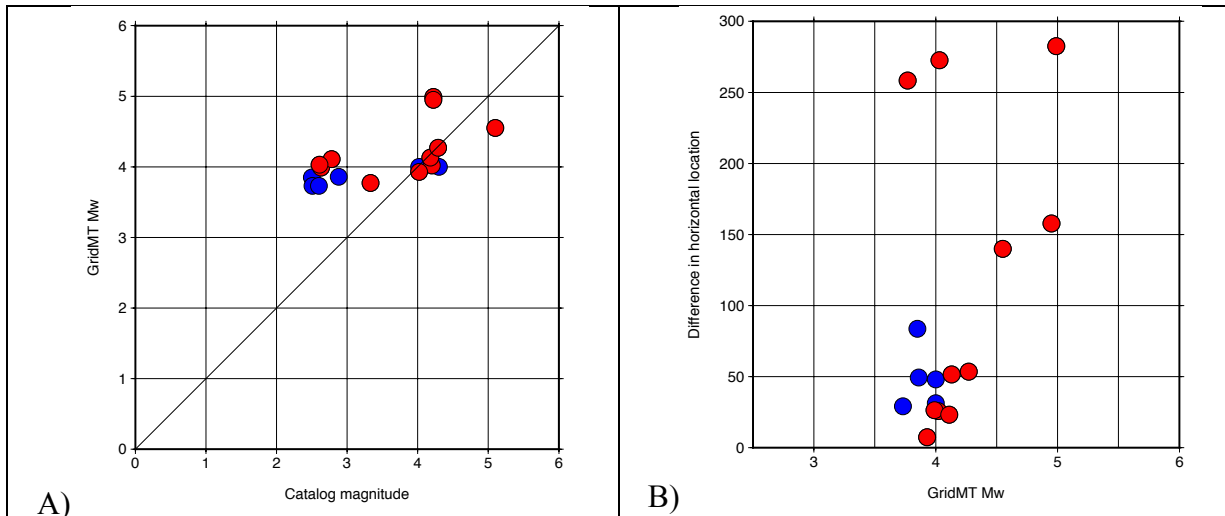


Figure 3. A) Comparison of GridMT Mw and catalog magnitude. The apparent saturation of GridMT Mw is in fact due to poor initial low magnitude estimates in the catalog for poorly located offshore events. B) Difference in location (km) vs. magnitude. There red circles are detections with a variance reduction greater than 60% and blue are less than 60%.

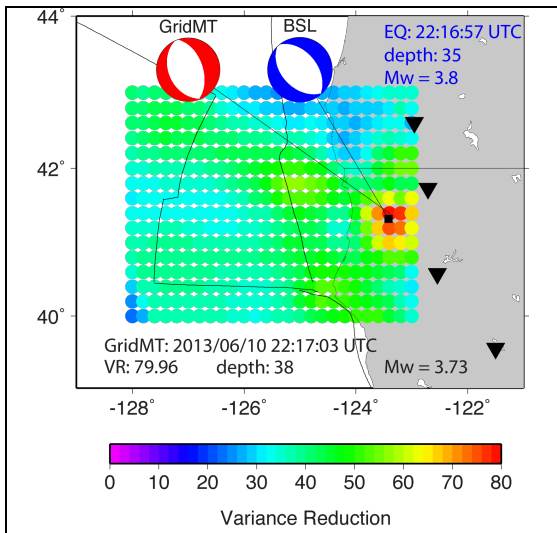


Figure 4. GridMT results for a Mw3.7 event that occurred on June 10, 2013.

Finally, Figure 4 gives an example of a well located Mw3.7 event that occurred recently on June 10, 2013. GridMT locates the event onshore at a depth of 38 km (the deepest depth allowed), which places it in the subducting Gorda plate. This location agrees well with the NCCS location and depth (35 km). The analyst reviewed focal mechanism is seen to agree well with the GridMT solution indicating a normal-slip mechanism, which likely results from flexure of the upper portion of the downgoing slab. In this case the preferred solution is the GridMT result because the goodness of fit parameter for the fitted velocity channels is nearly 80% where as the analyst reviewed solution using displacement data is only 38%. For this relatively low magnitude the integration of data from velocity to displacement

amplifies long-period noise significantly.

Summary

Through the course of this project we have refined GridMT software developed from a previous NEHRP grant, and have implemented it on an operational test bed. As described above the initial results are quite good, and we have already begun modifying the algorithm to improve performance, which will be an ongoing effort as we collect solutions on the test bed. The objective is to eventually migrate the method from the test bed to the operational environment.

Based on the success of the $M_w < 7.5$ implementation utilizing streaming velocity channels in the 0.02 to 0.05 Hz passband, we are now in the process of constructing the Green's functions matrices using the quasi-finite-source method (Guilhem et al., 2012) for the larger magnitude implementation. This implementation will operate on streaming acceleration data in the 0.005 to 0.01 Hz passband as demonstrated in Guilhem et al. (2012). The objective of this implementation is to develop a megathrust earthquake monitoring capability possibly providing for tsunami early warning. This implementation will be completed in July 2013, and our testing will be to analyze low frequency noise levels on possible false detection, and to refine the algorithm to reduce possible detections of teleseismic wavefields.

References

- Guilhem, A., and D. S. Dreger (2011). Rapid detection and characterization of large earthquakes using quasi-finite-source Green's functions in continuous moment tensor inversion, *Geophys. Res. Lett.*, Vol. 38, L13318, doi:10.1029/2011GL047550.
- Guilhem A., D. S. Dreger, H. Tsuruoka, and H. Kawakatsu (2012). Moment tensors for rapid characterization of megathrust earthquakes: the example of the 2011 M9 Tohoku-oki, Japan earthquake, *Geophys. Journ. Int.*, doi:10.1093/gji/ggs045.
- Guilhem, A., D. S. Dreger, P. Lombard (2013). GridMT in northern California: Preliminary results of continuous detection and characterization of earthquakes using moment tensors, *Seism. Res. Lett.*, 84:2, pg. 362.
- Kawakatsu, H., (1998) On the realtime monitoring of the long-period seismic wavefield., *Bull. Earth. Res. Inst.*, 73, 267-274.
- Tsuruoka, H., H. Kawakatsu, and T. Urabe (2009), GRiD MT (grid-based real-time determination of moment tensors) monitoring the long-period seismic wavefield, *Physics of the Earth and Planetary Interiors*, 175, 8-16, doi:10.1016/j.pepi.2008.02.014

Appendix

Guilhem and Dreger (2011) and Guilhem et al. (2012) as published in *Geophysical Research Letters* and *Geophysics Journal International*

Rapid detection and characterization of large earthquakes using quasi-finite-source Green's functions in continuous moment tensor inversion

Aurélie Guilhem¹ and Douglas S. Dreger¹

Received 23 March 2011; revised 25 May 2011; accepted 25 May 2011; published 15 July 2011.

[1] Large earthquakes along subduction zones have the potential to generate tsunamis along local coasts, as well as traveling far across oceans. By continuously inverting for moment tensors we show that it is possible with a single procedure to automatically detect, locate and determine source parameters of any earthquake, from magnitude 3.5 to larger than 8 located in both the near- and far-field. We find that the detection and characterization of large earthquakes is improved when quasi-finite-source Green's functions are used in a point-source moment tensor approach as they represent to some extent the rupture's finiteness and directivity. Solutions can be obtained within several minutes after the origin time of the earthquake, and could therefore be used as part of a near-source tsunami early warning system, capable of providing tens of minutes of possible warning depending on the distance of the earthquake rupture from the coast. **Citation:** Guilhem, A., and D. S. Dreger (2011), Rapid detection and characterization of large earthquakes using quasi-finite-source Green's functions in continuous moment tensor inversion, *Geophys. Res. Lett.*, 38, L13318, doi:10.1029/2011GL047550.

1. Introduction

[2] As recently demonstrated by the 2004 magnitude (Mw) 9.0 Sumatra, the 2010 Mw8.8 Chile and the 2011 Mw9.0 Japan seismic events, great subduction zone earthquakes are capable of triggering devastating, high-fatality tsunamis in their near field, in addition to producing intense local ground shaking [Bryant, 2001; Hirshorn and Weinstein, 2009]. With increasing continuously recording seismic networks, current efforts provide earthquake and tsunami early warnings within 5 to 10 min after the origin time [Lomax and Michelini, 2009]. Current procedures focus on earthquake location, depth, magnitude, and slowness [Hirshorn and Weinstein, 2009]. But initial tsunami early warning statements are commonly issued without knowing the focal mechanism of the earthquake, which has first order importance, together with the magnitude and focal depth, on the excitation of tsunami waves.

[3] Kanamori and Rivera [2008] proposed the use of the fast-propagating long-period W-phase in an automated manner for moment tensor inversions. Complete earthquake source parameters can be known within 20 minutes following the earthquake origin time [Kanamori and Rivera,

2008] and are now computed at the Pacific Tsunami Warning Center as well as in Japan [Tsuruoka *et al.*, 2009a]. However, it remains limited in its ability to provide useful near-field tsunami early warnings because of its intrinsic time delay [Lay *et al.*, 2005]. Considering datasets closer to the earthquake rupture may improve the processing time for the source characterization by putting a lower distance bound on the useable data. But the rupture dimensions for M8+ events violate the point-source assumptions applied in moment tensor inverse methods. Even if finite-source inversions solve this problem, their realtime implementations are computationally demanding [Dreger and Kaverina, 2000; Dreger *et al.*, 2005]. Also, while it is possible to rapidly obtain solutions within a 20 min time frame for M6+ offshore events [Dreger, 2010] the scaling of finite-source model dimensions for great earthquakes precludes their implementation in realtime. On the other hand, Kawakatsu [1998] proposed a realtime approach to automatically detect, locate and determine the source parameters of earthquakes occurring within a predefined region by computing moment tensors at each point of a grid from continuously streaming long-period (>10 sec) waveform data. With a limited number of stations and assuming a point-source representation, this method gives correct results in terms of detection and source characterization of up to M7 earthquakes offshore Japan [Tsuruoka *et al.*, 2009b].

[4] Here, we present an adapted version of Kawakatsu's [1998] method, focusing on the most seismically active region of northern California: the Mendocino Triple Junction (MTJ), where small to potentially tsunamigenic earthquakes occur. For major earthquakes (M8+), we propose a point-source moment tensor inversion that takes into account the finiteness of the rupture zone by constructing quasi-finite-source Green's functions (GFs). It becomes possible to monitor all $M > 3.5$ earthquakes with a direct procedure that autonomously detects, locates, and computes source parameters. This is performed using a single step procedure in contrast to the standard cascade-type analysis currently employed in northern California [Gee *et al.*, 2003].

2. Data and Method

[5] With approximately 80 earthquakes with magnitude larger than 3 every year, the MTJ is known as the most seismically active region in northern California [Oppenheimer, 2007]. Its seismicity is mostly located offshore: along the Mendocino Transform Fault (MTF), within the highly deformed Gorda plate, and along the Cascadia Subduction Zone (CSZ) (Figure 1). Paleoseismic evidence of great earthquakes along the CSZ [Atwater, 1987], including radiocarbon dating and several offshore turbidite

¹Berkeley Seismological Laboratory, University of California, Berkeley, California, USA.

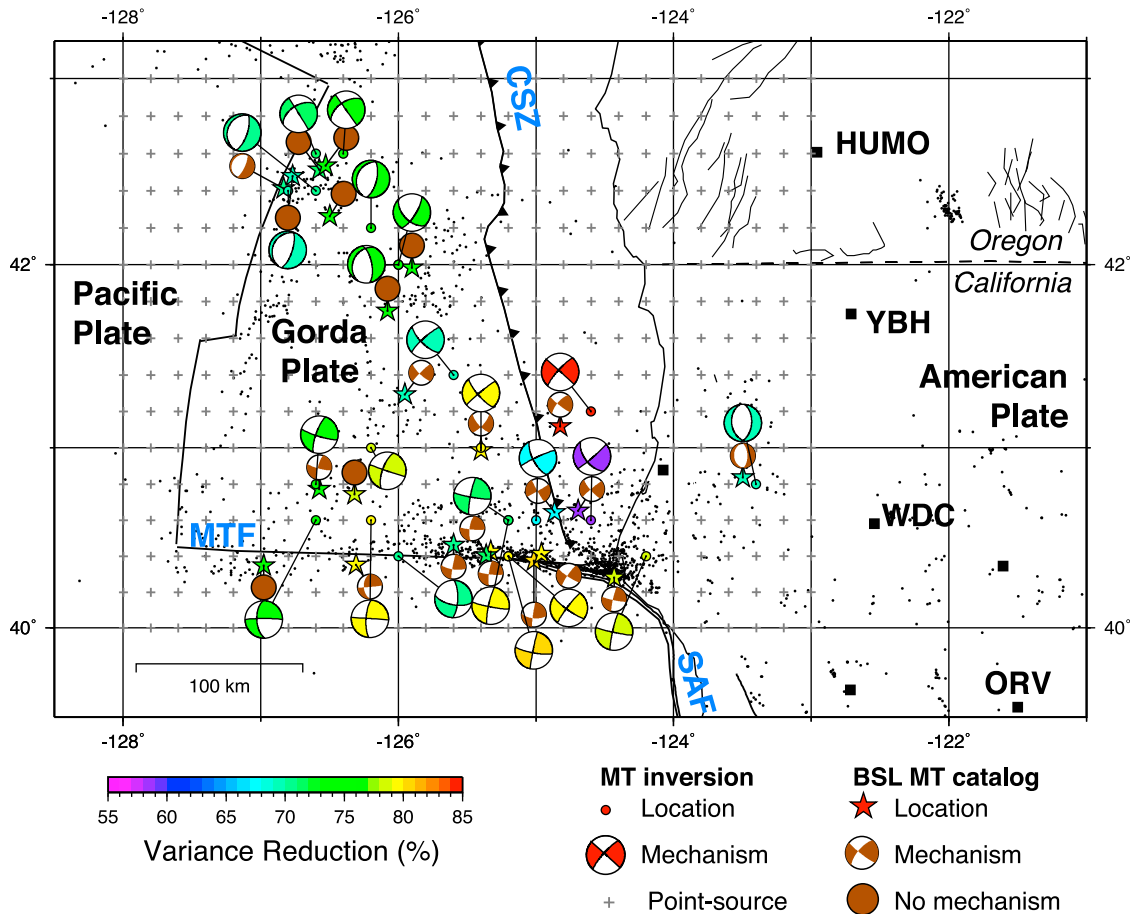


Figure 1. Map of the Mendocino Triple Junction region showing the grid of point sources (crosses). The four seismic stations used are HUMO, ORV, WDC and YBH. Black dots show the regional seismicity (M3+) since 1990. The studied events are shown in brown for the catalog solutions and are color-coded by the VR for the inversion solutions. CSZ, MTF, and SAF mark the Cascadia subduction zone, the Mendocino transform fault, and the San Andreas fault, respectively.

episodes of deformation in the last 2000 years [Clarke and Carver, 1992], indicate that the CSZ is capable of multiple M8+ earthquakes, as large as M9 [Goldfinger *et al.*, 2008; Satake *et al.*, 1996; Heaton and Hartzell, 1987].

[6] In northern California, current realtime earthquake monitoring is performed sequentially by the U.S. Geological Survey at Menlo Park and the Berkeley Seismological Laboratory [Gee *et al.*, 2003]. Because seismic stations are located onshore, poor azimuthal coverage of the seismic wave radiation patterns often leads to difficulties in detecting and locating events, and thus in determining their full source parameters. There is a need to implement a system that will automatically characterize earthquake sources and will not depend on the successful completion of multi-stage processing.

[7] Kawakatsu [1998] proposed to continuously invert the long period seismic wavefield (>10 sec) for moment tensors at grid points representing virtual sources distributed over a region. At each station, the data d are represented as the convolution of the GF tensor, G , describing the wave propagation between the source and the receiver, and the moment tensor components m of the source:

$$d = G \cdot m \quad (1)$$

[8] The least-square solution for the moment tensor can be obtained:

$$M = (G^T G)^{-1} G^T d \quad (2)$$

where the $(G^T G)^{-1} G^T$ matrix for each point-source can be computed in advance knowing a priori the grid distribution and the set of pre-selected seismic stations. The multiplication of this matrix with streaming data can be performed continuously as soon as the data arrives at a central site. Earthquake detection is given when the variance reduction (VR) exceeds a detection threshold:

$$VR = \left[1 - \frac{\sum_i \sqrt{(data_i - synth_i)^2}}{\sum_i \sqrt{data_i^2}} \right] \times 100 \quad (3)$$

where $data$, and $synth$ are the discrete data and GF time series, respectively, and the summation is performed for all stations and components.

[9] We propose to implement a moment tensor grid search covering the MTJ using four broadband seismic stations of the Berkeley Digital Seismic Network and nearly 5,000 virtual sources located every 0.2° in latitude and longitude and every 3 km in depth, between 5 and 38 km (Figure 1).

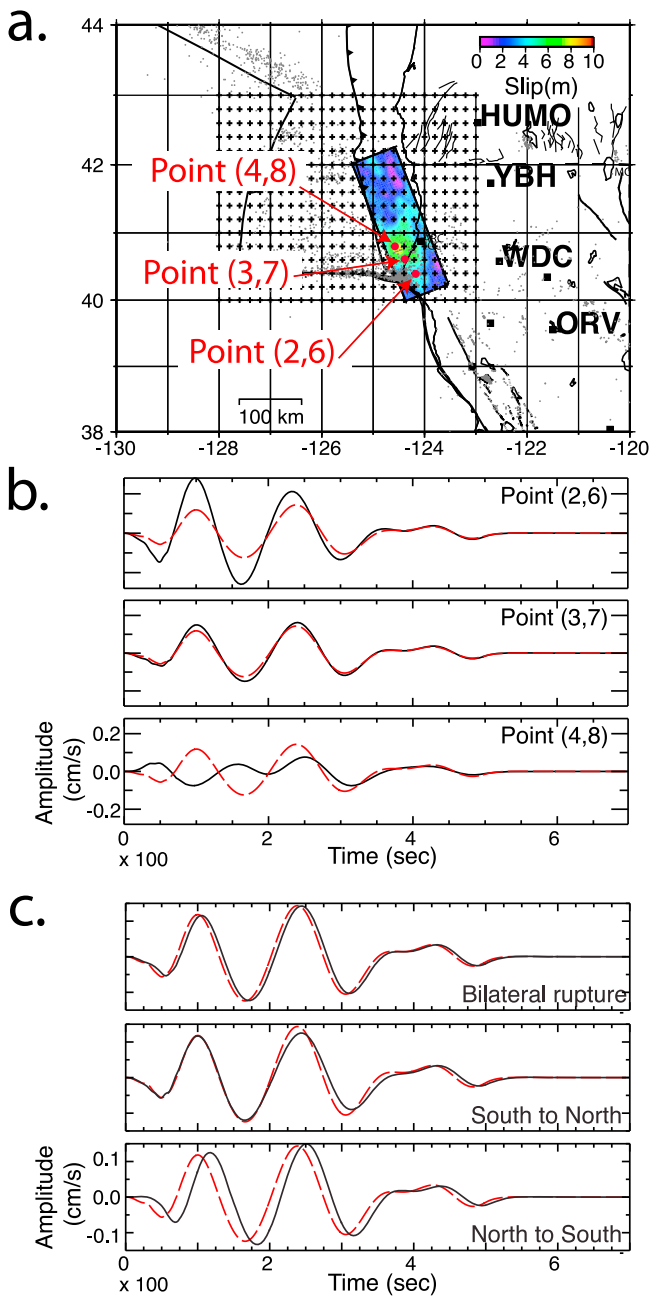


Figure 2. (a) Map of the slip model of a synthetic M8.1 earthquake (rectangle). Arrows point to the three grid-points considered in the generation of quasi-finite-source GFs. (b) Synthetic EW components at WDC computed for the three different grid-points (black, solid traces) compared to the quasi-finite-source GF computed using the three selected grid points (red, dashed traces). (c) Directivity in the quasi-finite-source GF (black, solid traces) compared to the GFs without directivity of Figure 2b (red, dashed traces).

We suggest running in parallel a system for small to moderate earthquakes and a second one for large (M8+) earthquakes along the CSZ (see auxiliary material).¹ For M3.5–7 earthquakes, the inversion of 380 sec of data is performed

¹Auxiliary materials are available in the HTML. doi:10.1029/2011GL047550.

every 2 seconds after filtering the seismic wavefield between 20 and 50 sec. This allows sufficient propagation time for the full seismic waveforms to reach the seismic stations. For the second system, we invert a longer record (i.e., 480 sec) and filter the data between 100 and 200 sec (Figure S1). In addition, for large earthquakes, the source time function becomes a significant parameter that needs to be considered. We choose to include an 84-sec source time function to the GFs corresponding to the synthetic M8.2 earthquake we present here (Figures 2 and S1), however it is possible to consider several different source time function durations within a reasonable range for scenarios targeting specific types of events (e.g., Mw 8.0, 8.5, 9.0, etc.).

[10] For M8+ earthquakes along the CSZ, we propose to invert for moment tensors only at the grid points that are distributed in the slab. This significantly lowers the number of calculations and permits us to focus on the most hazardous region of the grid. It is then possible to consider earthquake scenarios in advance and to invert for them in realtime. However, this grows into a near-field problem in which the stations are sensitive to different parts of the overall rupture. We propose here to employ quasi-finite-source adjusted GFs where GFs of n grid points are averaged in advance to generate composite GFs, G_{tot} , that take into account the source-receiver back-azimuth and thereby the effective radiation patterns of each component (Figure 2):

$$G_{tot}(t) = \sum_{i=1}^n G_i(t) / n \quad (4)$$

[11] The prefixed number of points n has an effect on the complexities of the pre-defined earthquake scenarios considered in the realtime inversions. Directivity can also be pre-included in the composite GFs, giving constraints on the nature of finite rupture (i.e., unilateral or bilateral) (Figure 2):

$$G_{tot}(t) = \left[G_1(t) + \sum_{i=2}^n G_i(t) \cdot \left(\frac{\Delta_{1-n}}{v_r} \right) \right] / n \quad (5)$$

where Δ_{1-n} is the distance between Source 1 (reference source) and Source n and v_r is the rupture velocity. The moment tensor inversion itself is performed assuming a point-source analysis method, which maintains the computational speed. One of the point-sources of the composite GF is considered as a reference because information about the corresponding azimuths between the selected grid-point and the seismic stations is needed to rotate the GFs into the East, North and vertical components for the realtime inversion.

3. Results

[12] We test the concept on M4 to M7.1 earthquakes (Figure 1 and Table S1). The solutions obtained using a 1 D velocity model agree well with the Berkeley moment tensor catalog solutions confirming that this system is suitable for implementation in the MTJ region. However, the 20–50 sec inversions of 380 sec long records for a synthetic M8.2 reverse event with uniform slip fail to recover the earthquake parameters, yielding only Mw 6.7 and a poor fit, VR = 47% (Figure S1). Because of the narrow band processing, the point-source inversion only fits a small part of the record and is not sensitive to the total seismic moment. The source

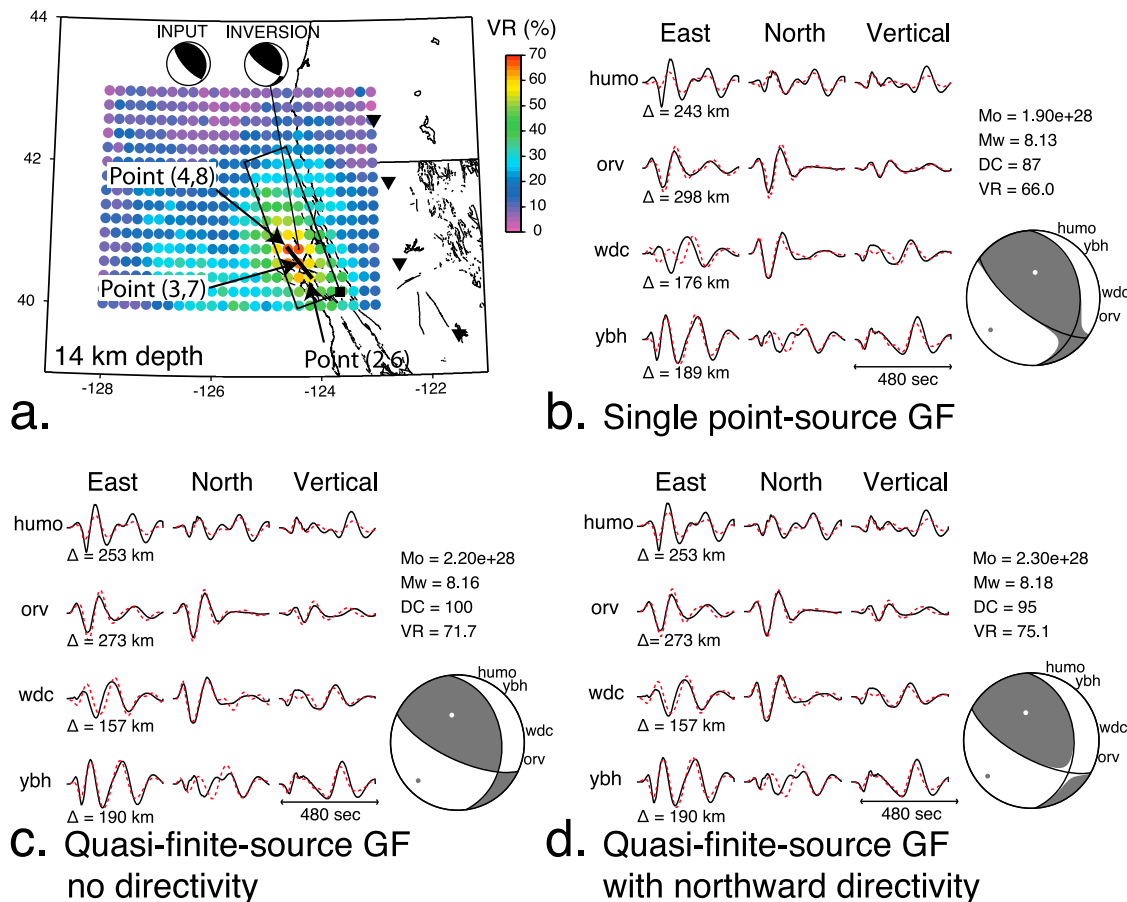


Figure 3. (a) Map of the best VRs at 14 km depth obtained for a point-source moment tensor inversion for a synthetic M8.2 earthquake (rectangle). The best mechanism (top right) is compared to the input mechanism (top left). Arrows point to the points that are considered in the multi-point source inversion. (b) Best moment tensor solution obtained at Point (3,7). (c) Moment tensor solution for the multi-point source inversion (no directivity). (d) Moment tensor solution for the multi-point source inversion with a northward directivity.

corner frequency of the event (~ 0.011 Hz) is indeed lower than the frequency band considered. In contrast, the 100–200 sec passband works better (VR = 54.6% in Figure S1) and gives a point-source location near the fault centroid, the correct Mw and focal mechanism. Similar results are also obtained for a variety of slip models (Mw8.2 and 8.4) using a single point-source moment tensor inversion with point-source GFs (Figures 3a, 3b, and S2). As Figure 3 shows, the best solution obtained for a synthetic M8.2 earthquake with variable slip is found within the rupture segment near the centroid. We find that more realistic variable slip distributions are better represented by a point-source assumption at longer periods as proposed by *Fukuyama and Dreger* [2000].

[13] We show that it is possible to improve the fit between the synthetics and the data (Figure 3c) after simultaneously summing the GFs of several grid points centered on the event centroid. Figure 3d shows that, by considering a northward rupture in the composite GFs and a rupture velocity of 3 km/sec, the corresponding earthquake solution has a larger VR and better estimates the focal parameters (Table S2). Similar results are obtained for a M8.4 synthetic seismic event, which presents an extended rupture (i.e., 480 km) and two major slip areas (Figure S2). This method permits raising the detection level of large earthquakes and allows us to obtain more precise

source parameters (Table S2), by considering a range of quasi-finite-source Green's functions for different directivity scenarios and source time duration.

4. Discussion and Conclusion

[14] We show that it is possible to detect and characterize the seismic activity of the MTJ region using an algorithm that performs moment tensor inversions using streaming waveform data. The powerful addition of quasi-finite-source GFs enables better definition of the centroid location, the correct source mechanism and magnitude of large earthquakes. Used in a point-source formalism, they allow more rapid detection of major events and more precise determination of their source parameters than is likely to be available using standard processing systems. This approach may enable applications for tsunami early warning in the near-field of large coastal earthquakes. Detections from the automated moment tensor inversion can be as fast as the length of the inverted seismic records. Complete earthquake information is retrieved about 6 minutes after a M4–7 earthquake and 8 minutes after a M8+ earthquake. To this time, data telemetry latency (~ 2 sec) and a negligible ($\ll 1$ sec) delay for filtering and resampling need to be added as well as

a few tens of seconds to assess fit and determine a maximum in the VR [Tsuruoka *et al.*, 2009b].

[15] In the open ocean, the velocity of tsunami propagation is proportional to the water depth. Depending on the distance of the area of uplift from the coast, the open-ocean transit times for tsunami waves may be about 6 to 20 minutes. However, the actual transit time is likely to be closer to 20 minutes due to decreasing water depth, and as reported after an Mw7.1 earthquake in 1992 that occurred at Cape Mendocino [Oppenheimer *et al.*, 1993]. Its largest amplitudes, from an edge wave, arrived 3 hours after the event [Gonzalez *et al.*, 1995]. The devastating tsunami waves following the 2011 Mw9.0 Japan earthquake arrived about 20–30 minutes after the rupture (Japan Meteorological Agency, The 2011 off the Pacific coast of Tohoku earthquake, 2011, available at http://www.jma.go.jp/jma/en/2011_Earthquake.html). The method we propose may allow for tens of minutes of warning in the near-field.

[16] Strong motion data of the 2011 M9.0 Japan earthquake reveals that 100–200 sec accelerations can be recorded with high signal-to-noise levels with modern instrumentation (Figure S3). After adapting G. Shao *et al.*'s (Preliminary result of the March 11th, 2011 Mw9.1 Honshu earthquake, 2011, available at http://www.geol.ucsb.edu/faculty/ji/big_earthquakes/2011/03/0311_v3/Honshu.html) slip model of the M9.0 Japan event for the MTJ region, we find good detection and characterization of the earthquake with VRs up to 85% (Figures S3 and S4). Finally, seismic instrumentation could clip from the strong shaking of a large local/regional earthquake. One or several near-field stations could also be rendered non-operational at the time of the earthquake affecting the algorithm performance. Overcoming this issue is possible by using secondary seismic stations or only a subset of the stations. However this could affect the VRs and lead to a non-detection (Figures S5 and S6). High-rate continuous GPS data could also provide on-scale observations for even the largest earthquakes [Larson *et al.*, 2003; Avallone *et al.*, 2011]. Using adequately calibrated velocity models and a proper grid distribution, this grid search approach can be implemented to include both seismic and geodetic datasets in any region that experiences intense and potentially tsunamigenic seismic activity.

[17] **Acknowledgments.** Supported by the U.S. Geological Survey through external award G10AP00069. We thank Robert Uhrhammer, GRL editor Ruth Harris, reviewer Barry Hirshorn and an anonymous reviewer for their constructive advices. Strong motion data of the 2011 M9.1 Japan earthquake from the K-NET, National Research Institute for Earth Science and Disaster Prevention (NIED). Berkeley Seismological Laboratory contribution 11-02.

References

Atwater, B. F. (1987), Evidence for Great Holocene earthquakes along the outer coast of Washington State, *Science*, *236*, 942–944, doi:10.1126/science.236.4804.942.

Avallone, A., *et al.* (2011), Very high rate (10 Hz) GPS seismology for moderate-magnitude earthquakes: The case of the Mw6.3 L'Aquila (central Italy) event, *J. Geophys. Res.*, *116*, B02305, doi:10.1029/2010JB007834.

Bryant, E. (2001), *Tsunami: The Underrated Hazard*, 350 pp., Cambridge Univ. Press, New York.

Clarke, S. H., and G. A. Carver (1992), Late Holocene tectonics and paleoseismicity, southern Cascadia Subduction zone, *Science*, *255*(5041), 188–192, doi:10.1126/science.255.5041.188.

Dreger, D. S. (2010), January 10, 2010 Mw6.5 Gorda Plate earthquake: Automated finite-source modeling, annual report, Berkeley Seismol. Lab., Berkeley, Calif. [Available at http://seismo.berkeley.edu/annual_report/ar09_10/node23.html.]

Dreger, D., and A. Kaverina (2000), Seismic remote sensing for the earthquake source process and near-source strong shaking: A case study of the October 16, 1999 Hector Mine earthquake, *Geophys. Res. Lett.*, *27*, 1941–1944, doi:10.1029/1999GL011245.

Dreger, D. S., L. Gee, P. Lombard, M. H. Murray, and B. Romanowicz (2005), Rapid finite-source analysis and near-fault strong ground motions: Application to the 2003 Mw 6.5 San Simeon and 2004 Mw 6.0 Parkfield earthquakes, *Seismol. Res. Lett.*, *76*(1), 40–48, doi:10.1785/gssrl.76.1.40.

Fukuyama, E., and D. Dreger (2000), Performance test of an automated moment tensor determination system for the future “Tokai” earthquake, *Earth Planets Space*, *52*, 383–392.

Gee, L., D. Neuhauser, D. Dreger, M. Pasyanos, R. Uhrhammer, and B. Romanowicz (2003), The Rapid Earthquake Data Integration System, in *International Handbook of Earthquake and Engineering Seismology, Int. Geophys. Ser.*, vol. 81, pp. 1261–1273, Academic, Amsterdam.

Goldfinger, C., *et al.* (2008), Late Holocene rupture of the northern San Andreas Fault and possible stress linkage to the Cascadia Subduction Zone, *Bull. Seismol. Soc. Am.*, *98*, 861–889, doi:10.1785/0120060411.

Gonzalez, F. I., K. Satake, E. F. Boss, and H. O. Mofjeld (1995), Edge wave and non-trapped models of the 24 April 1992 Cape Mendocino Tsunami, *Pure Appl. Geophys.*, *144*, 409–426, doi:10.1007/BF00874375.

Heaton, T. H., and S. H. Hartzell (1987), Earthquake hazards on the Cascadia Subduction Zone, *Science*, *236*, 162–168, doi:10.1126/science.236.4798.162.

Hirshorn, B., and S. Weinstein (2009), Earthquake source parameters, in *Encyclopedia of Complexity and Systems Science*, Pt. 5, pp. 2657–2676, doi:10.1007/978-0-387-30440-3_160.

Kanamori, H., and L. Rivera (2008), Source inversion of W phase: Speeding up seismic tsunami warning, *Geophys. J. Int.*, *175*, 222–238, doi:10.1111/j.1365-246X.2008.03887.x.

Kawakatsu, H. (1998), On the realtime monitoring of the long-period seismic wavefield, *Bull. Earthquake Res. Inst. Univ. Tokyo*, *73*, 267–274.

Larson, K. M., P. Bodin, and J. Gombert (2003), Using 1 Hz GPS data to measure deformations caused by the Denali Fault earthquake, *Science*, *300*, 1421–1424, doi:10.1126/science.1084531.

Lay, T., *et al.* (2005), The Great Sumatra-Andaman earthquake of 26 December 2004, *Science*, *308*, 1127–1133, doi:10.1126/science.1112250.

Lomax, A., and A. Michelini (2009), Tsunami early warning using earthquake rupture duration, *Geophys. Res. Lett.*, *36*, L09306, doi:10.1029/2009GL037223.

Oppenheimer, D. (2007), Mendocino Triple Junction offshore northern California, Woods Hole Sci. Cent., U.S. Geol. Surv., Woods Hole, Mass. [Available at http://woodshole.er.usgs.gov/operations/obs/rmobs_pub/html/mendocino.html.]

Oppenheimer, D., *et al.* (1993), The Cape Mendocino, California, earthquakes of April 1992: Subduction at the Triple Junction, *Science*, *261*, 433–438, doi:10.1126/science.261.5120.433.

Satake, K., K. Shimizaki, Y. Tsuji, and K. Ueda (1996), Time and size of a giant earthquake in Cascadia inferred from Japanese tsunami records of January 1700, *Nature*, *379*, 246–249, doi:10.1038/379246a0.

Tsuruoka, H., L. Rivera, H. Kawakatsu, and H. Kanamori (2009a), Real-time source inversion using W-phase and GRiD MT for regional tsunami early warning, *Eos Trans. AGU*, *90*(52), Fall Meet. Suppl., Abstract S13A-1732.

Tsuruoka, H., H. Kawakatsu, and T. Urabe (2009b), GRiD MT (grid-based real-time determination of moment tensors) monitoring the long-period seismic wavefield, *Phys. Earth Planet. Inter.*, *175*, 8–16, doi:10.1016/j.pepi.2008.02.014.

D. S. Dreger and A. Guilhem, Berkeley Seismological Laboratory, University of California, 225 McCone Hall, Berkeley, CA 94720-4670, USA. (aurelie@seismo.berkeley.edu)

Moment tensors for rapid characterization of megathrust earthquakes: the example of the 2011 M 9 Tohoku-oki, Japan earthquake

Aurélie Guilhem,^{1,2} Douglas S. Dreger,¹ Hiroshi Tsuruoka³ and Hitoshi Kawakatsu³

¹Berkeley Seismological Laboratory, University of California Berkeley, Berkeley, CA 94720-4760, USA. E-mail: aurelie@seismo.berkeley.edu

²Swiss Seismological Service, ETH Zurich, NO H66, Sonneggstrasse 5, 8092 Zürich, Switzerland

³Earthquake Research Institute, University of Tokyo, 1-1-1 Yayoi, Bunkyo-ku, Tokyo 113-0032, Japan

Accepted 2012 October 23. Received 2012 October 8; in original form 2011 December 2

SUMMARY

The rapid detection and characterization of megathrust earthquakes is a difficult task given their large rupture zone and duration. These events produce very strong ground vibrations in the near field that can cause weak motion instruments to clip, and they are also capable of generating large-scale tsunamis. The 2011 M 9 Tohoku-oki earthquake that occurred offshore Japan is one member of a series of great earthquakes for which extended geophysical observations are available. Here, we test an automated scanning algorithm for great earthquakes using continuous very long-period (100–200 s) seismic records from K-NET strong-motion seismograms of the earthquake. By continuously performing the cross-correlation of data and Green's functions (GFs) in a moment tensor analysis, we show that the algorithm automatically detects, locates and determines source parameters including the moment magnitude and mechanism of the great Tohoku-oki earthquake within 8 min of its origin time. The method does not saturate. We also show that quasi-finite-source GFs, which take into account the effects of a finite-source, in a single-point source moment tensor algorithm better fit the data, especially in the near-field. We show that this technique allows the correct characterization of the earthquake using a limited number of stations. This can yield information usable for tsunami early warning.

Key words: Earthquake source observations; Seismic monitoring and test-ban treaty verification; Early warning.

1 INTRODUCTION

The great M 9 Tohoku-oki earthquake that struck offshore of Japan on 2011 March 11 caused very strong ground shaking, with a recorded maximum ground acceleration reaching nearly $3 \times g$. It ruptured a region extending several hundred kilometres and produced peak velocity of 1 m s^{-1} (Okada 2011). The main shock also generated a large tsunami on the local and regional coastlines with run-up heights reaching 37.9 m (Lay *et al.* 2011; Mori *et al.* 2011). The significant tsunami was experienced throughout the Pacific basin. This event followed a sequence of other great subduction zone earthquakes like the 2004 M 9.2 Banda Aceh and the 2010 M 8.8 Maule earthquakes, that became notorious for their large scale tsunamis (Lay *et al.* 2005; Vigny *et al.* 2011; Yamazaki & Cheung 2011). These three earthquakes demonstrate the need to rapidly detect and correctly characterize seismic events from both near- and far-field observations. The analysis of near-field/regional-distance observations is an important contribution toward developing a local tsunami warning capability.

Data from continuously recording and telemetered seismic networks help to rapidly provide earthquake and tsunami warnings as soon as an earthquake's location and magnitude are known. However, great earthquakes pose a series of significant problems for tsunami warning purposes. First, the amplitudes of the seismic waves can exceed the dynamic range of the broadband and weak motion seismic instruments typically used for earthquake detection and location in the local and regional distance range. The use of strong motion instrumentation, or even continuous GPS estimates of dynamic ground motions can alleviate this problem (Clinton & Heaton 2002; Blewitt *et al.* 2009; Yue & Lay 2011). Secondly, great earthquakes have extended rupture areas along the subduction plane and last up to several minutes for the largest events. Traditional rapidly applied earthquake characterization techniques are not formulated to consider their long period waves (i.e. not above 50 s periods for example). Consequently they rely on information at frequencies above the corner frequency of these large events and therefore suffer saturation problems. This leads to the underestimation of the seismic moment and magnitude of the events.

In the case of the $M 9$ Tohoku-oki earthquake, the Japanese Meteorological Agency (JMA) first announced the magnitude of the event as 7.9 (Okada 2011). Magnitude updates progressively published by the JMA finally reached magnitude 9.0 on 2011 March 13. Similarly, the United States Geological Survey (USGS) initially announced a $M 7.9$ for the event (Hayes *et al.* 2011), and the first bulletin of the Pacific Tsunami Warning Center (PTWC) reported the same magnitude (PTWC 2011).

The use of far-field seismic stations is common for tsunami early warning purposes as they can provide accurate information regarding the earthquake (Kanamori & Rivera 2008). However, while the utilization of the far-field stations enables warnings for teleseismic distances, warnings for local and regional coastlines remains an issue due to the time it takes for the seismic waves to travel to the far-field stations. In addition, because the extent of rupture in these great earthquakes is finite, common local and regional distance point-source techniques may suffer from oversimplification of the Green's functions (GFs) and the computational demands of a full finite-source inversion technique. Finally, initial tsunami early warnings based on teleseismic observations are commonly issued without knowing the type of earthquake rupture (Hirshorn & Weinstein 2009; Lomax & Michellini 2009), which can have significant effects on the generation and amplitudes of the tsunami waves.

Kanamori & Rivera (2008) proposed an automated moment tensor inversion scheme using the very long period W-phase that travels between the P and S waves at teleseismic distances. The main advantage of this method is that it can provide complete earthquake source parameters, and an unsaturated estimate of scalar moment within 20 min of an earthquake using far-field stations. At the time of the 2011 $M 9$ Tohoku-oki earthquake, the W-phase source inversion algorithm was running in real-time (Duputel *et al.* 2011). In contrast to other techniques the reports from the use of the W-phase announced that the earthquake magnitude was 8.8–9.0 within the 40 min of the origin time (Duputel *et al.* 2011). These results show that it is possible to rapidly detect and characterize the source parameters of large earthquakes, however the solution was too late to provide useful tsunami early warnings for the local coastlines. The initial low-amplitude tsunami waves were followed 20–30 min after the event's origin time by the damaging tsunami waves. Their arrival was still within the 40 min processing time of the W-phase method (Duputel *et al.* 2011; Hayashi *et al.* 2011; Okada 2011).

Kawakatsu (1998) proposed the GRiD MT method to automatically detect, locate and determine the source parameters of any earthquake by inverting long-period (>10 s) seismic waveforms and computing moment tensors in real-time at each point of a grid covering a region of interest. Although this approach was successfully implemented in Japan and has given good results in terms of detection, location and characterization of the offshore seismicity for up to $M_w 7$ (Tsuruoka *et al.* 2009a), and an effort to combine it with the W-phase method was in progress (Tsuruoka *et al.* 2009b), it failed to detect the $M 9$ earthquake as the broad-band records of the F-NET network were clipped in the strong shaking of the $M 9$ main shock. Running the GRiD MT algorithm on strong-motion data streams avoids this problem. Guilhem & Dreger (2011) implemented the GRiD MT method for the Mendocino Triple Junction region, and suggested modifying the approach by considering two GRiD MT algorithms running in parallel. One is similar to that currently used in Japan (Tsuruoka *et al.* 2009a). The other is for characterizing large earthquakes (i.e. $M > 7$). In the latter case, longer period waveforms (i.e. 100–200 s) are considered, and a longer time window (i.e. about 8 min) is employed, so that the full wavefield including Rayleigh and Love waves can reach a limited

number of seismic stations located at distances of several hundred kilometres. Using synthetic $M 8$ – $M 9$ earthquakes, Guilhem & Dreger (2011) showed that this approach can be used to correctly detect great earthquakes, locate them and obtain their magnitude and mechanism. In addition, to properly account for the finiteness of the rupture of great earthquakes, they proposed the use of quasi-finite-source (QFS) GFs to account for the finite extent of great earthquake ruptures in the point-source moment tensor inversion method.

Here, we use strong-motion data from the $M 9$ Tohoku-oki main shock recorded by the K-NET network to test the approach proposed by Guilhem & Dreger (2011). We present the results of the single point-source moment tensor inversions using data from sets of four seismic stations. Fukuyama & Dreger (2000) proposed the use of 50–200 s period to correctly recover scalar moment in great earthquakes, and here we use longer periods (i.e. between about 100 and 200 s period) to better approximate a point-source for megathrust events. We show that this method can correctly characterize the event without magnitude saturation about 8 min after its origin time. We also present tests using QFS GFs representing several case scenarios of ruptures and slip directions. In addition, to retrieve the correct source parameters of the great earthquakes, this approach uses a limited amount of calculations compared to the more general application, by focusing the grid on the megathrust contact patch, and as a result it demonstrates its potential for real-time implementation in Japan as well as in other regions where great earthquakes occur. However, we find that some strong-motion stations show non-linearity in their signal, which emphasizes the need to better understand the behaviour of strong motion instruments and recording sites under strong ground shaking (i.e. tilt or other potential issues). We also discuss the importance of station configuration to enhance the detection and characterization of such events. Used in real-time, this method could allow at least 10 or more minutes of warning for tsunami waves, and would improve estimates of tsunami size based on the moment magnitude and mechanism of the earthquake.

2 DATA AND METHOD

2.1 Method

We modified the GRiD MT method proposed by Kawakatsu (1998) and used by Tsuruoka *et al.* (2009a), based on Guilhem & Dreger's (2011) recommendations. The GRiD MT approach considers the continuous inversion for the moment tensors of streaming real-time data at each point of a grid that represent virtual sources distributed over a region. Guilhem & Dreger (2011) showed that, in order to correctly characterize large earthquakes (i.e. $M_w > 7$) the algorithm needs to focus on very long period data (for example, between 100 and 200 s compared to 20 and 50 s periods) over a longer time window in order to sample the flat part of the spectrum proportional to moment. At each station, the data d^k (k denoting the vertical, north–south and east–west components) can be represented directly as the convolution of GFs or elementary seismograms, G , between the source, s and the receiver, r , and the moment tensor components m of the source

$$d^k(t) = \sum_i G_i^{sr}(t) m_i^s, \quad (1)$$

where the sum is carried out over the fundamental components of the moment tensor: m_{xx} , m_{xy} , m_{xz} , m_{yy} , m_{yz} , m_{zz} (e.g. Jost & Hermann 1989). The least-squares solution to this representation

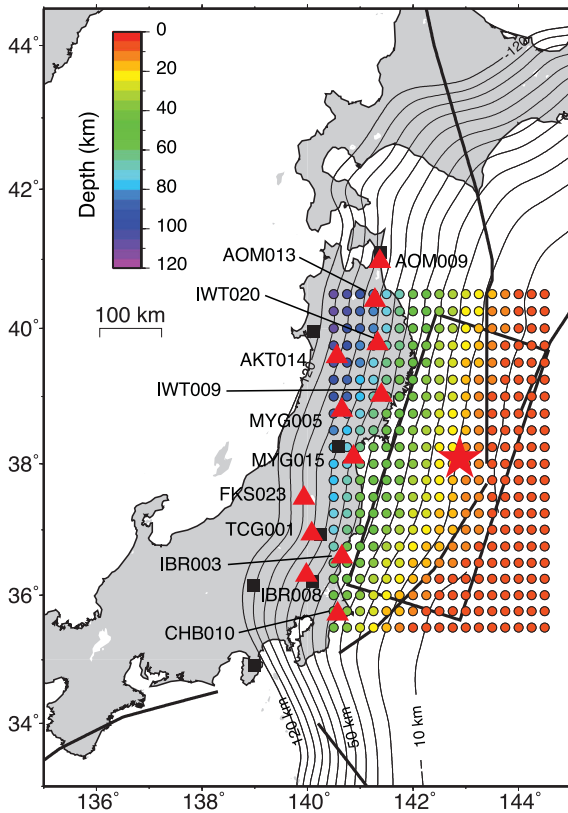


Figure 1. Gridpoint (dots) colour-coded by the depth of the slab (Hayes & Wald 2009) and K-NET strong-motion stations (triangles) compared with the locations of the broad-band stations (squares) used by Tsuruoka *et al.* (2009a). The star shows the JMA epicentre of the $M9$ Tohoku-oki earthquake and the rectangle shows the extension of its slip according the model of Shao *et al.* (2011).

can be obtained by computing the generalized inverse $(G^T G)^{-1} G^T$ and solving for the moment tensor M

$$M = (G^T G)^{-1} G^T d. \quad (2)$$

The generalized inverse $(G^T G)^{-1} G^T$ can be pre-computed *a priori* using a distribution of gridpoints, a given velocity model and a set of selected stations. The multiplication of this matrix with streaming data can be performed automatically in real-time. Earthquake detection is given when the variance reduction (VR), or fit between the data and the synthetic seismograms exceeds a predefined threshold. With a limited number of stations and assuming a point-source representation, this method gives correct results in terms of detection and source characterization for up to $M7+$ earthquakes in the Mendocino Triple Junction region offshore northern California (Guilhem & Dreger 2011) and offshore Japan (Tsuruoka *et al.* 2009a).

This original method offers several advantages. It gives the possibility to: (1) use multiple data sets (displacement, velocity or acceleration seismograms), (2) consider various earthquake scenarios in advance and to invert for them in real-time and (3) incorporate the effects of 3-D structure through the use of pre-computed GFs that are virtual-source-station specific. Guilhem & Dreger (2011) demonstrated that in addition to computing simple point-source inversions, it was possible to employ QFS GFs where GFs of n gridpoints are pre-averaged to generate composite GFs, G_{tot} , that take into account the source-receiver back-azimuth and thereby the effective radiation patterns of each virtual source:

$$G_{\text{tot}}(t) = \sum_{i=1}^n \frac{G_i(t)}{n}. \quad (3)$$

The prefixed number of points n has an effect on the allowed complexity of the pre-defined earthquake scenarios considered in the real-time inversions. This allows us to take into consideration the near-field problem in which the stations are sensitive to different parts of the overall rupture, with or without directivity. The moment

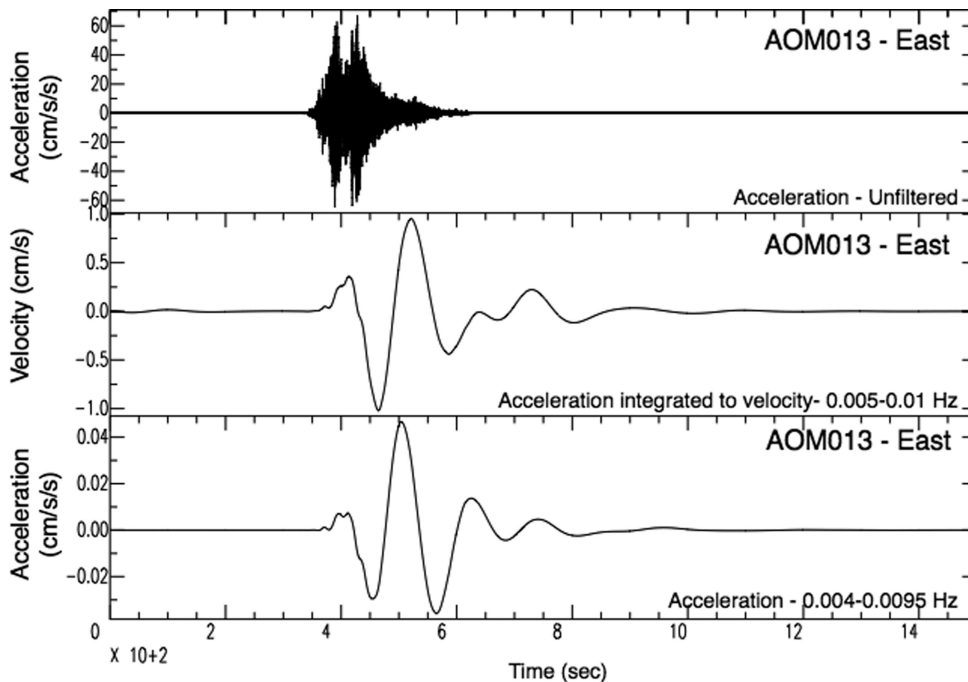
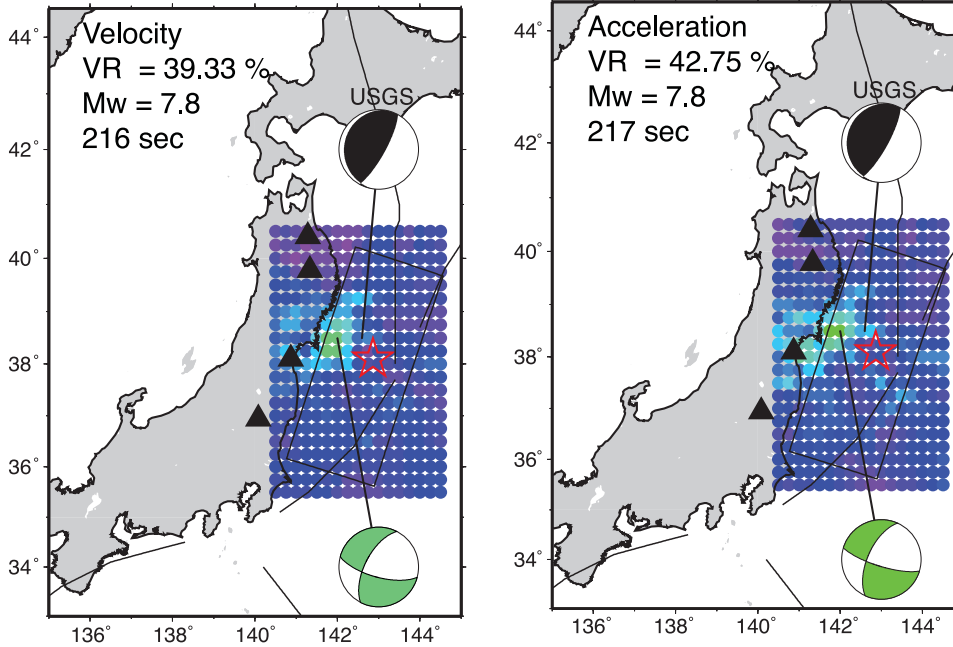


Figure 2. Waveform comparison at the East component of station AOM013. Top: raw, unfiltered strong-motion data. Middle: top seismogram integrated to velocity and bandpass filtered between 0.005 and 0.01 Hz. Bottom: top seismogram bandpass filtered between 0.004 and 0.0095 Hz.

a. 20-50 sec period



b. 100-200 sec period

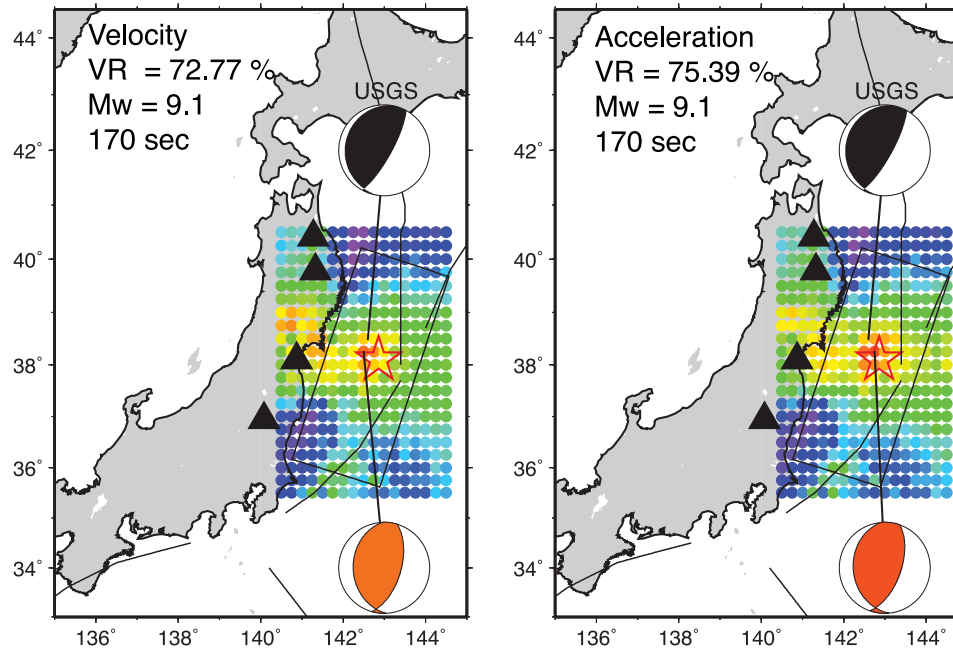


Figure 3. Maps of the best variance reductions per gridpoints (dots) obtained ± 5 km from the slab depth using the data of four strong motion stations (triangles) integrated to velocity (left-hand panels) and let as acceleration (right-hand panels). (a) Inversions using data filtered between 20 and 50 s period. (b) Inversions using data filtered between about 100 and 200 s. The best double-couple solution is shown by the coloured beach-ball diagram and is compared with the USGS CMT mechanism (black). The red star shows the JMA epicentre. Origin time in second is given with respect to the starting time of the inversion: 05:44:02 UTC.

tensor inversion itself is performed assuming a point-source analysis method, which maintains the computational speed. It is noted that if a specific target were sought it would be possible to simply convolve the streaming data against GFs that take the specific strike, rake and dip of the target event into account. We have elected to retain the inversion capability for these parameters since in addition to the megathrust events large intraplate earthquakes that rupture the slab are also possible. Finally, we invert the deviatoric decomposition of the moment tensors by imposing a zero trace constraint on the inversion. Even though the use of full GFs for a full moment tensor inversion is possible, it is not critically needed for the fast identification and characterization of great earthquakes.

2.2 Data

The dense seismic networks (F-NET, K-NET, Hi-NET) of the Japanese National Research Institute for Earth Science and Disaster Prevention (NIED) provide a remarkable data set of geophysical observations of the M 9 Tohoku-oki earthquake. The GRiD MT algorithm implemented in Japan by Tsuruoka *et al.* (2009a) uses a subnet of three stations of the broad-band network F-NET for each of their processing grids. Analysis of these data shows that they went off-scale and suffered other linearity issues following the earthquake and they are not usable. On the other hand, strong-motion stations are less vulnerable to clipping (Clinton & Heaton 2002). The strong-motion K-NET network in Japan has nearly 700 three-component stations distributed almost every 25 km and recording at 100 samples per second (sps), and it offers the opportunity to study the Tohoku-oki event in detail. We selected 12 of these stations because of (1) their location along the rupture of the M 9 Tohoku-oki earthquake, (2) their location adjacent to the F-NET stations used by Tsuruoka *et al.* (2009a) and (3) because they recorded a minimum of 300 s of data (Fig. 1). This last condition was necessary to assure that most of the seismic signal from the main shock was taken into account and to provide sufficient recording for the long-period moment tensor analysis (i.e. 100–200 s period). Similarly to the currently implemented GRiD MT in Japan (Tsuruoka *et al.* 2009a) and to the method proposed by Guilhem & Dreger (2011), we use multiple combinations of four stations each. This is a rather limited number of stations for a source analysis but this is a necessary condition for the fast computation of the moment tensors on a

grid of point sources required for a near real-time application. Tests of the solidity of the results are mentioned later.

Because the proposed approach considers a minimum of 8 min of streaming data, and because the K-NET instruments are event-triggered and records are only a few minute long, we extended the available acceleration seismograms by adding zeros before and after the data segment to that we could stream the data through the algorithm in the same manner as it would be applied with continuous streaming data. In this way, we generated 20-min time-series that were later processed before entering the streaming data moment tensor algorithm. Adding zeros was possible because of the large signal-to-noise ratios of the data.

Similarly to what is currently implemented in Japan (Tsuruoka *et al.* 2009a,b) and to what was proposed by Guilhem & Dreger (2011) who used velocity data, we integrated the acceleration records to obtain their equivalent in velocity. We then filtered them using a one-pass, two-pole Butterworth bandpass filter, and we decimated the data to 1 sps. Integration is a relatively unstable process in the presence of long-period noise. Such noise can be greatly amplified through the integration process, and can result in biases in the inversion results. This is also true of instrument deconvolution, and therefore in application it will be desirable to process raw streaming data, and account for instrument response by applying the appropriate response function to the GFs. For these reasons we decided to utilize the data in the native unit of the sensors. Therefore we also considered the acceleration records in the moment tensor inversion, and we compared the results from the two inversions. The 20-min acceleration segments were filtered with a one-pass, three-pole Butterworth bandpass filter at 0.004 (250 s) and 0.0095 (105 s). This filter passband was chosen after comparing the acceleration data with that integrated to velocity (Fig. 2).

2.3 Grid and GFs

We implemented a grid of virtual sources extending between latitudes 35.5°N and 40.5°N and between longitudes 140.5°E and 144.5°E at intervals of 0.25° and overlapping the rupture of the M 9 earthquake (Fig. 1). Because great earthquakes, including the 2011 M 9 Tohoku-oki earthquake, primarily rupture the subduction interface we implemented a grid of virtual sources distributed on

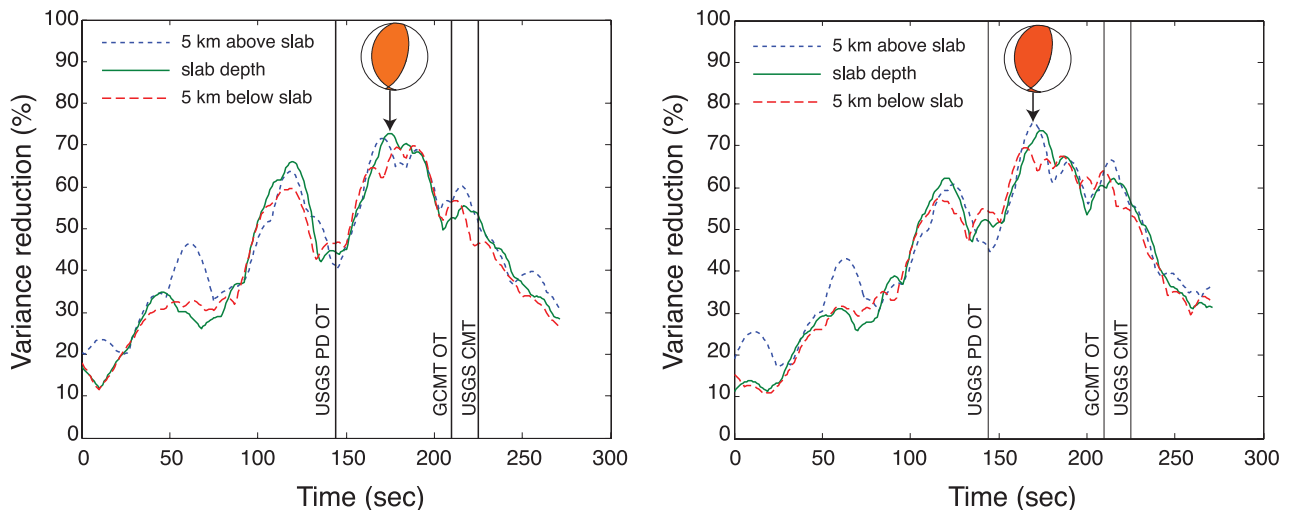
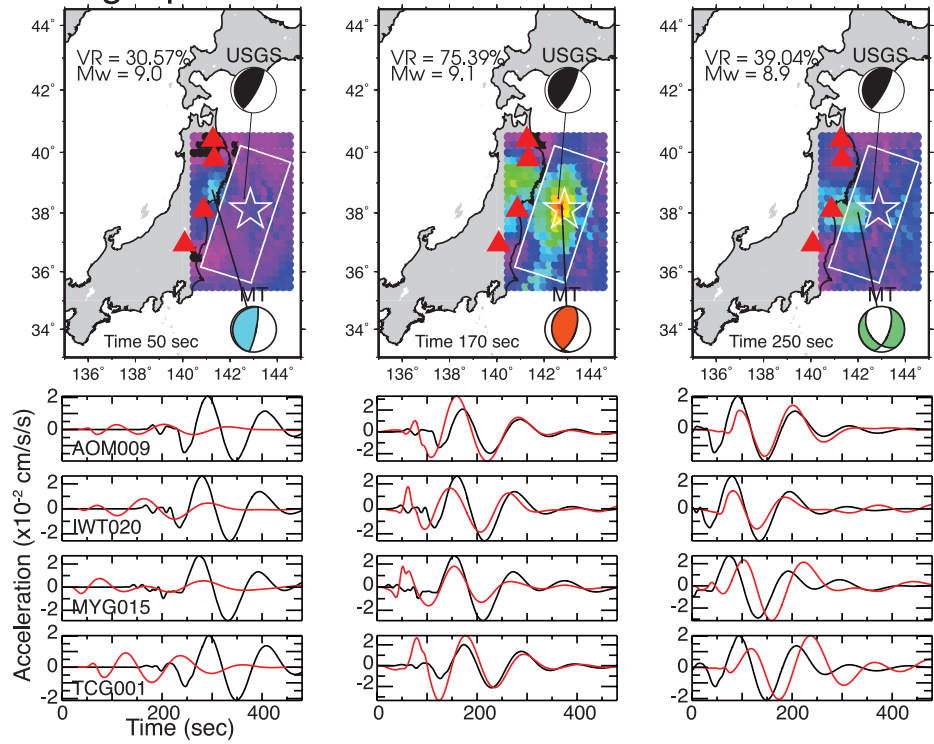


Figure 4. Temporal evolution of the maximum variance reductions for the velocity (left-hand panel) and acceleration (right-hand panel) inversions over the grid. The beach-balls show the best solutions (Fig. 3). Inversions start at time 05:44:02 UTC (0 s) and run for about 4.5 min, every second.

a. Single point source



b. Quasi-finite-source

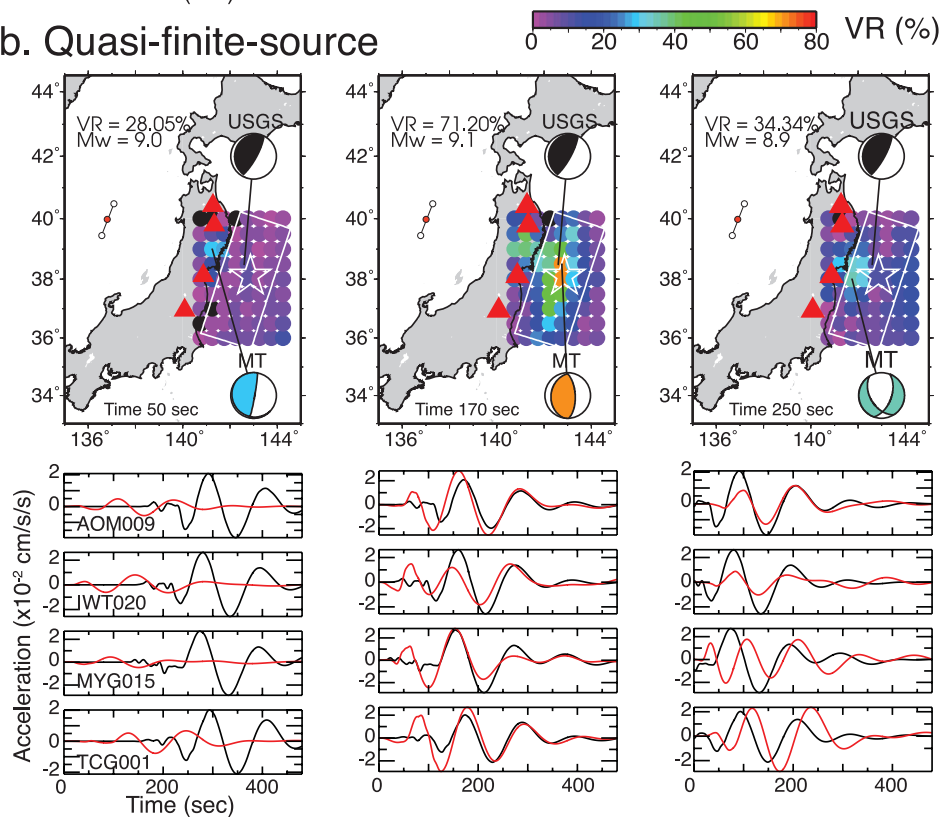


Figure 5. Detection and waveform comparisons at times 50, 170 and 250 s (170 s being the time of the best detection) for the single-point-source inversions (a) and for the quasi-finite-source inversions (b) using three points simultaneously. Seismic waveforms (vertical component) are aligned from north to south and show the observed data (black) and the best synthetic waveforms (red) corresponding to the best solution for each time step shown in the maps.

a slab. The slab geometry followed that of Kamchatka, the Kurils and Japan from the 3-D compilation of subduction zone geometries Slab1.0 (Hayes & Wald 2009). We discretized the slab depth with a 5 km spacing. The depths considered range between 5 and 115 km (Fig. 1).

We pre-computed a catalogue of GFs and their associated generalized inverse matrices $(G^T G)^{-1} G^T$ using the 1-D velocity model used by Tsuruoka *et al.* (2009a) in their implementation of GRiD MT. We used a frequency–wavenumber integration code (FKRPROG) written by Chandan Saikia (1994), based on the method of Wang & Herrmann (1980) to compute the velocity GFs at the depth of the interpolated slab as well as 5 km shallower and 5 km deeper. It is important to use a complete wavefield method to compute the GFs to properly account for near- and intermediate-field terms considering the long-period passband and near-regional distance range. To account for the inversion of acceleration data we differentiated the velocity GFs to acceleration before to applying identical filters to those used for the strong-motion records. Finally, because of the long rupture duration of great earthquakes, the elementary seismograms were generated and convolved with different Brune (1970) source time functions in the pre-processing stage of the analysis. We present here results with a source time duration of 100 s and Table 2 regroups the results for different source time functions (discussed later).

3 DETECTION USING SINGLE-POINT-SOURCE GFS

We find that when data and elementary seismograms are filtered between 20 and 50 s period the method using a point-source approximation fails to return the correct magnitude and mechanism of the earthquake (Fig. 3a). This can be explained by the proximity of the stations to the rupture segment and the frequency band being above the corner frequency of the event. However, the method utilizing the same stations but long-period waveforms (at and above the earthquake’s corner frequency) and single-point-source inversions is able to correctly detect, locate and determine the source characteristics (seismic moment and mechanism) of the great M 9 Tohoku-oki earthquake (Fig. 3b), as compared with the W-phase solution and GCMT. It works for both acceleration records and velocity seismograms obtained from the strong-motion records. A maximum VR greater than 70 per cent was obtained using either velocity or acceleration records.

The best solutions in both of the two long-period tests are located near the centroid of the earthquake, close to the JMA and USGS CMT locations. Like the CMT solution, the mechanism obtained is reverse with the strike direction approximating the slab orientation in this location. In contrast to other traditional source determination techniques, the approach does not saturate at large magnitudes and

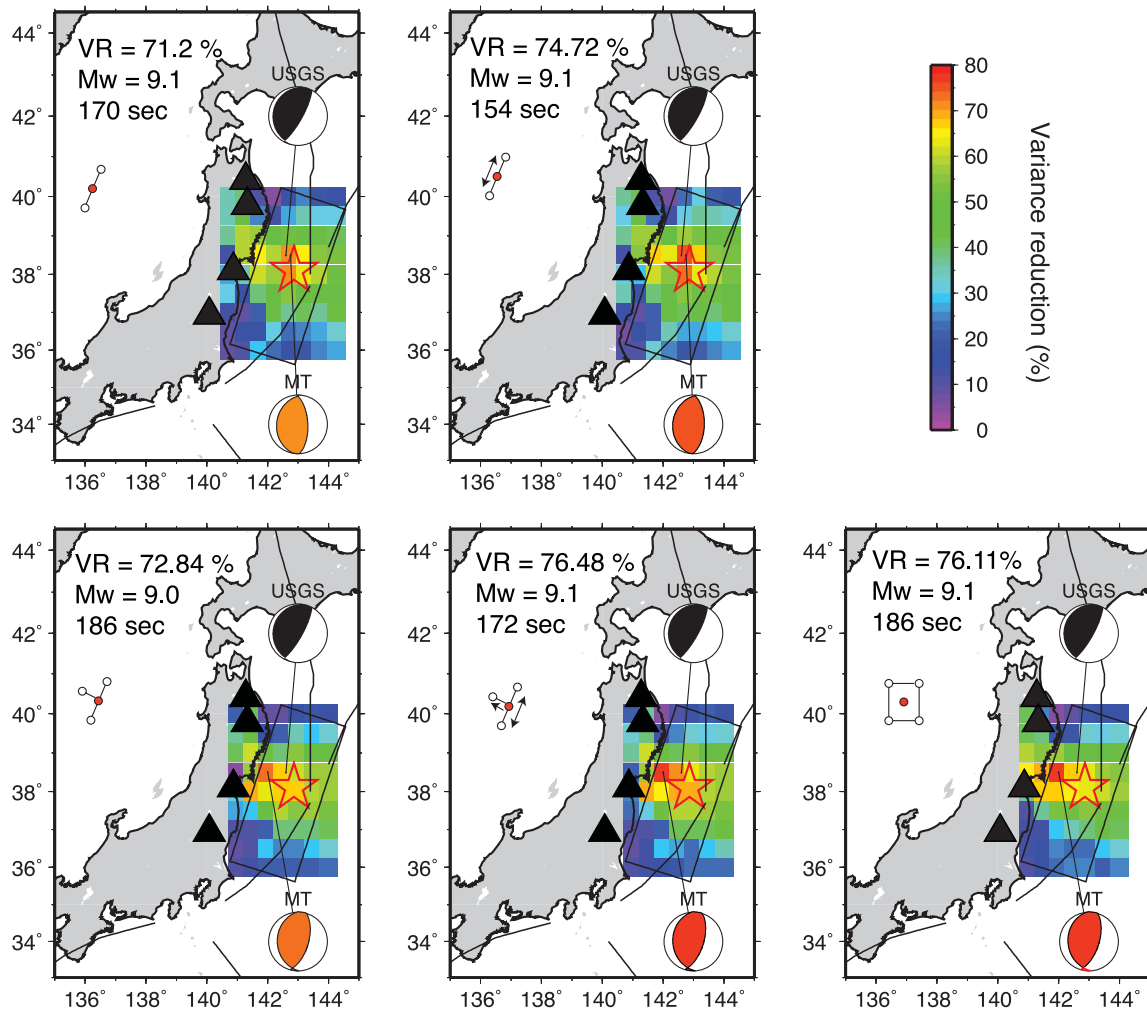


Figure 6. GRiD MT results for acceleration records at four stations (triangles) at slab depth using different quasi-finite-source GFs shown by the white and red dots representing the combination of point sources (drawn to scale) with or without directivity (arrows). The red dots are considered as references for the rotations from transverse/radial components to east/north components and for the moment tensor inversions. See Fig. 3 for additional description.

Table 1. Effects of directivity on the moment tensor inversion for the three-point case (Fig. 6). Time is indicated in second from the start of the inversion at 05:44:02 UTC.

Rupture	VR (per cent)	Lat	Lon	M_w	Strike1	Rake1	Dip1	Strike2	Rake2	Dip2	Time (s)
No directivity	71.2	38.5	142.75	9.1	357	84	63	190	102	28	170
South to north	59.39	37.5	142.75	9.2	161	45	56	42	137	54	140
North to south	74.12	38	142.75	9.2	38	109	67	177	53	29	148
Bilateral	74.72	38.5	142.75	9.1	357	84	63	190	102	28	170

recovers a moment magnitude of 9.1, which is only 0.1 magnitude unit larger than the reported for this earthquake.

The method keeps pace with real-time streaming data but runs 8 min behind to ensure that the complete waveforms have been recorded by the most distant stations, and to capture the very long-period waves. The origin time of the earthquake was determined to be 05:46:42 UTC for the acceleration case (160 s after the start time of the inversion in Fig. 4), and 7 s later for the velocity inversion case (05:46:49 UTC or 167 s in Fig. 4). These origin times are within the range of origin times published for the event (05:46:23 UTC for the USGS catalogue to 05:47:47 UTC for the USGS CMT solution). Fig. 4 shows the temporal evolution of the best VRs calculated every second on the grid at the slab depth, 5 km above and 5 km below. In general, the VRs are found to be at or below 20 per cent before the earthquake time, even when the later part of those 8-min windows required in the inversion show evidence of the early arrivals of the earthquake. With time, the VRs increase until reaching a maximum value and then decrease rapidly once the wavefield passes through the time window of analysis. This is similar to what was observed by Tsuruoka *et al.* (2009a) and Guilhem & Dreger (2011) for small to large earthquakes in Japan and in northern California. Nonetheless, we notice the presence of peaks of higher VRs with a periodicity of approximately 100 s that we interpret as cycle shifting of the mechanism in which alternate peaks and troughs are fit as the data streams through the algorithm. This effect needs to be taken into account when scanning for the best VR and thus for defining the best solution, especially if the VRs are at or above the VR threshold. Fig. 5(a) shows the waveform fits obtained at three different time steps of the analysis.

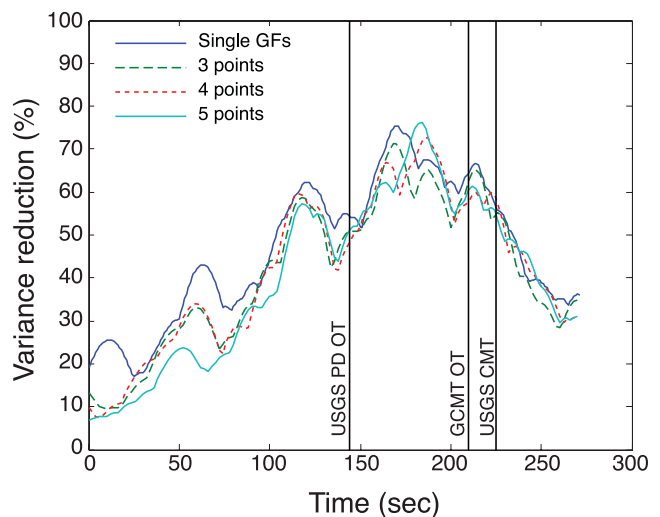
4 DETECTION USING QFS GFS

For great earthquakes, Guilhem & Dreger (2011) proposed the use of QFS GFS to account for the rupture finiteness at short distances. We tested a series of QFS GFS that represent to some extent the extended dimensions of the rupture in which we can also choose to add or not to add directivity with a rupture velocity fixed at 3 km s⁻¹ (Fig. 6). Here, we summed three, four and five gridpoints to create a series of rupture scenarios with elongated or square shaped QFS GFS. We chose to consider gridpoints distributed at the slab depth whose alignment corresponded to the general strike orientation of the slab, and whose spatial extents were relatively similar to the area of maximum slip during the rupture. More elongated and complex geometries for the construction of the QFS GFS are possible however they require prior knowledge of the characteristics of rupture, which is usually not the case, as they need to be defined before any near real-time inversions. Here, we search for the best VR every 2 s. This reduces the number of calculations for each time step from 1071 to 63. This number is also greatly reduced from the typical implementation in which the grid defines a 3-D volume (e.g. Tsuruoka *et al.* (2009a) and Guilhem & Dreger (2011)) rather than a region surrounding the subduction zone contact path. Typical

uniform implementations use 5000–7000 grid nodes, thus the QFS case with nodes only along the contact patch reduces the number of calculations per time step by a factor of 100.

We find that the use of this limited number of QFS GFS applied to strong-motion records allow the rapid detection of the M 9 Tohoku-oki earthquake with VRs exceeding 70 per cent and reaching a maximum of nearly 77 per cent (Figs 5b and 6). The mechanism, location and origin times are generally well recovered, and are similar to those obtained with the single-point-source GFS. This is due to the very compact nature of this great earthquake compared to other recent events (Lay *et al.* 2005; Vigny *et al.* 2011; Yamazaki & Cheung 2011). In addition, when using a bilateral rupture or a North to South rupture (Table 1), we better recover the source parameters of the earthquake (i.e. larger VR) as we better represent the actual rupture characteristics of the main shock in which finite-fault models of the event indicate that the earthquake first ruptured the shallow portion of the slab near its epicentre and later propagated along slab strike direction and also downdip (Ammon *et al.* 2011; Lay *et al.* 2011; Shao *et al.* 2011; Yue & Lay 2011).

Because this approach is less computationally intensive with the restricted number of inversions required, it is possible to invert simultaneously for several rupture models (i.e. multiple QFS structures with and without directivity, and use of different source time durations) in order to better reflect the range of anticipated ruptures in a region of interest. Furthermore, if additional constraints are available specific rupture scenarios may be tested in the same way. In fact, it would be possible to extend this approach to consider true finite source cases simply by testing the cross-correlation of those cases. It is noted however that it is presently not possible to invert for full finite-source models given the 8-min,

**Figure 7.** Comparison of the temporal evolution of the VRs for the GRiD MT using acceleration with single-point-source GFS (blue) and with QFS GFS from Fig. 6 (without directivity).

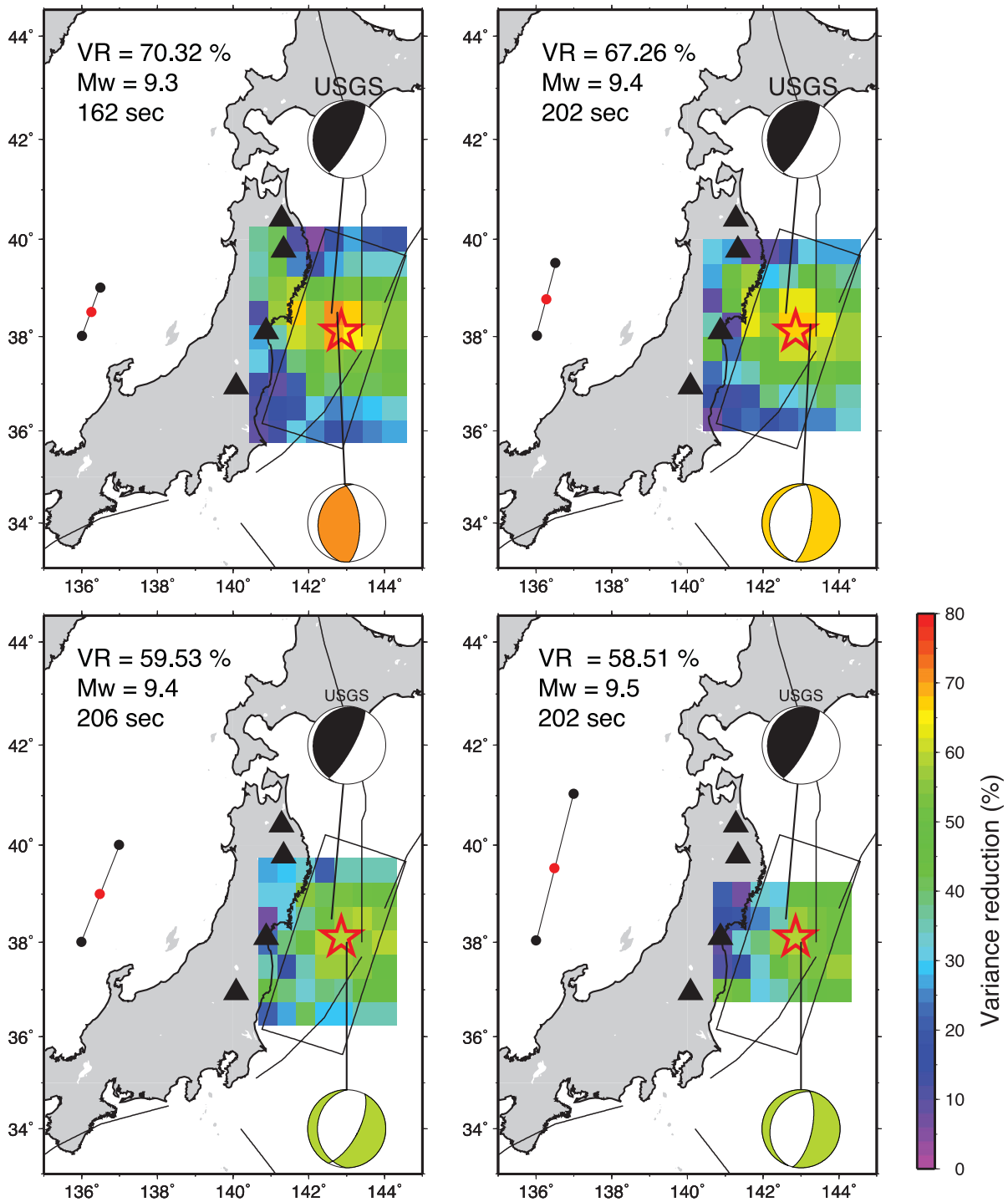


Figure 8. Effect of the increasing length of the QFS GFs on the GRiD MT capability to detect the $M 9$ Tohoku earthquake. The QFS GFs are built using three point sources (black and red dots) and the moment tensor analysis is performed using the position of the centre point (red dots), every 0.5° in latitude and longitude.

real-time processing time frame, and considering the additional degrees of freedom, increased uncertainty and uniqueness issues of such analyses. In any case, Fig. 6 demonstrates that very simple rupture scenarios with only three points can be used for the rapid characterization of this earthquake, which is similar to results from Guilhem & Dreger's (2011) tests for large earthquakes on faults with longer ruptures along the Cascadia Subduction Zone.

These results show that at long periods it is possible to detect and characterize a megathrust earthquake with a limited number of source inversions and with limited knowledge of the regional structure, earthquake rupture and duration using near-regional observations. Nonetheless, it is likely that additional tests will be necessary to better calibrate the filters, the GFs and the baseline noise characteristics for each region of monitoring interest. The results show that the proposed method can help to provide information that could be

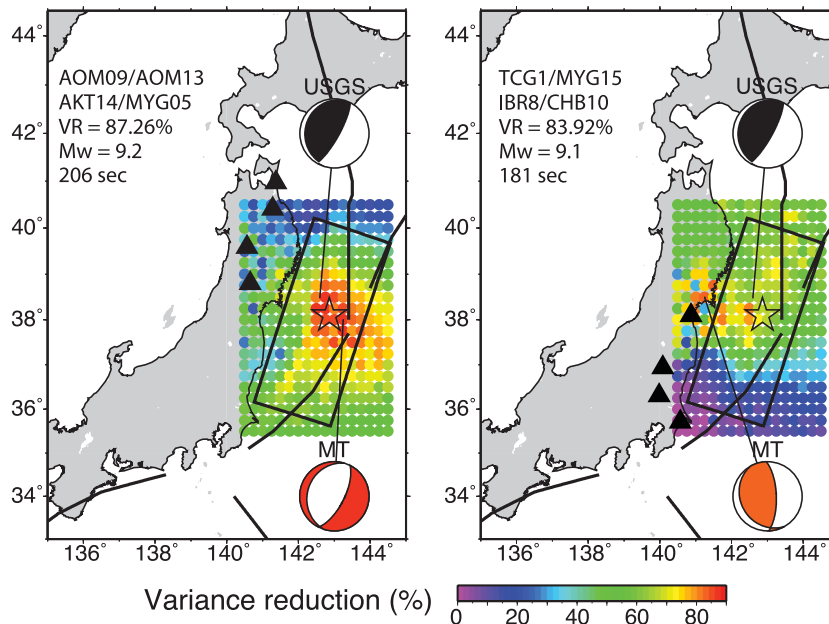


Figure 9. GrID MT results obtained with different station configurations: stations located in the northern part of the rupture (left-hand panel) and in the southern part of the rupture (right-hand panel).

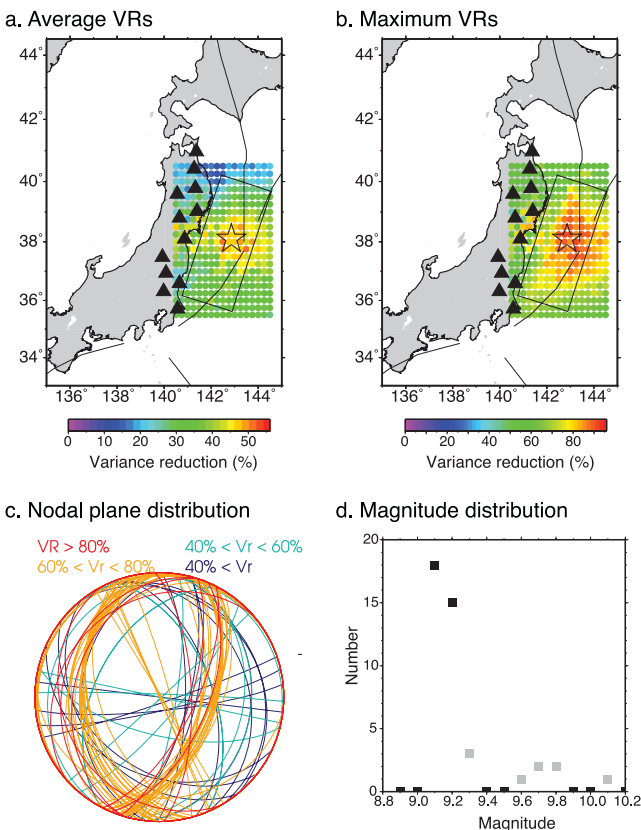


Figure 10. Results of 42 inversions using point-source approximation and different sets of four stations distributed along the rupture, in its northern end, and in its southern end. (a) Map view of the average VRs for each point of the grid. (b) Map view of the maximum VRs for each point. (c) Distribution of the nodal planes obtained for each 42 tests colour-coded by their VR. (d) Distribution of the magnitudes obtained for each test. The grey squares show the overestimated magnitudes obtained when stations shown in Fig. 11 are used.

utilized for tsunami early warning within minutes after a large earthquake. Finally, the temporal evolution of the VRs when considering QFS GFs is similar to that observed with the single-point-source analysis (Fig. 7). The VRs increase until reaching a maximum value and then decrease afterwards. We notice however that the VRs measured prior to the earthquake origin time are slightly lower for the QFS GFs than they are for the single-point-source test. This could be due to the single depth section considered in the later test compared to the results for three depths for the first one.

Even if no major difference is found in the change of the VRs over time (Fig. 7), these results show that using QFS GFs helps to enhance the system’s ability to detect a large earthquake by reducing computational demands. Of course a future M_w 9 event may be more distributed in nature than the Tohoku-oki earthquake with several asperities. The QFS GFs would in such cases improve the performance of the proposed system. Nonetheless, the design of the QFS GFs using more or less distant source points has direct effects on the capability of the system to detect the M_w 9 earthquake (Fig. 8). Although the location is found to remain stable, using only three points with increasing separation for the generation of QFS GFs progressively decreases the VRs from 70 per cent to about 58 per cent (Fig. 8) as the assumed rupture exceeds the actual main slip zone of the earthquake. The mechanism is also affected and we obtain here a normal fault solution at a later time corresponding approximately to the GCMT origin time (Fig. 8). We interpret the time delay and the opposite focal mechanism as the results of phase shifting in the streaming algorithm. Nonetheless, because the proposed approach significantly reduces the computational demands for a single run, it permits the search for multiple predefined rupture geometries in parallel (Fig. 7). The large VRs obtained for several of these models add confidence in the occurrence of large earthquakes despite the larger number of source parameters, in addition to the solutions obtained from other earthquake early warning systems. However, further tests are required in order to understand which solution(s) better detect the earthquake, and their relative timing.

5 DISCUSSION AND CONCLUSION

An appropriate grid arrangement and station configuration is important in order to correctly retrieve robust results. Fig. 9 shows that the location of the seismic stations considered in the inversions has an effect on the results, but in each of the cases it shows that location and magnitude are reasonably well constrained. In the case where the station subnet is to the north, the nodes with highest VR shift to the south (the opposite is seen for the southern subnet). This setting does not recover the correct mechanism (i.e. normal faulting event and rotated fault planes). However, it should be noted that the moment magnitude is 9.2 with a very high VR. Based on these two values there could still be some benefit for local/regional tsunami early warning systems. This solution is obtained at a later time and

corresponds to a phase shifting that could be better controlled if information from static offsets from GPS stations for example were included in the analysis. Sensitivity tests demonstrate that it is important to have a subnet of stations that span the expected rupture dimensions of the target earthquake. Additional tests were done with 42 different station distributions (Fig. 10). On average, we find that the M 9 Tohoku-oki earthquake could have been detected, with a correct estimation of its centroid, magnitude and fault motion orientation (Fig. 10). Exceptions to these results were obtained when the station distribution is narrow, and/or when stations that did not behave properly (see later) were considered, in which cases the magnitude estimates were larger than the true magnitude for lower VRs (Figs 9 and 10).

Table 2. Effect of the source time duration on the moment tensor algorithm using acceleration data for the main shock.

Source duration (s)	Lat	Lon	Time (s)	M_w	Strike1	Rake1	Dip1	Strike2	Rake2	Dip2	VR (per cent)
25	38.25	142.75	193	8.8	20	102	61	176	69	31	65.53
50	38.35	142.75	183	8.9	21	103	61	175	67	31	71.96
100	38.25	142.75	170	9.1	19	102	61	175	69	31	75.39
150	38.25	142.75	163	9.2	17	101	62	175	71	30	74.61
200	38.25	142.75	158	9.3	16	100	61	176	72	30	72.39

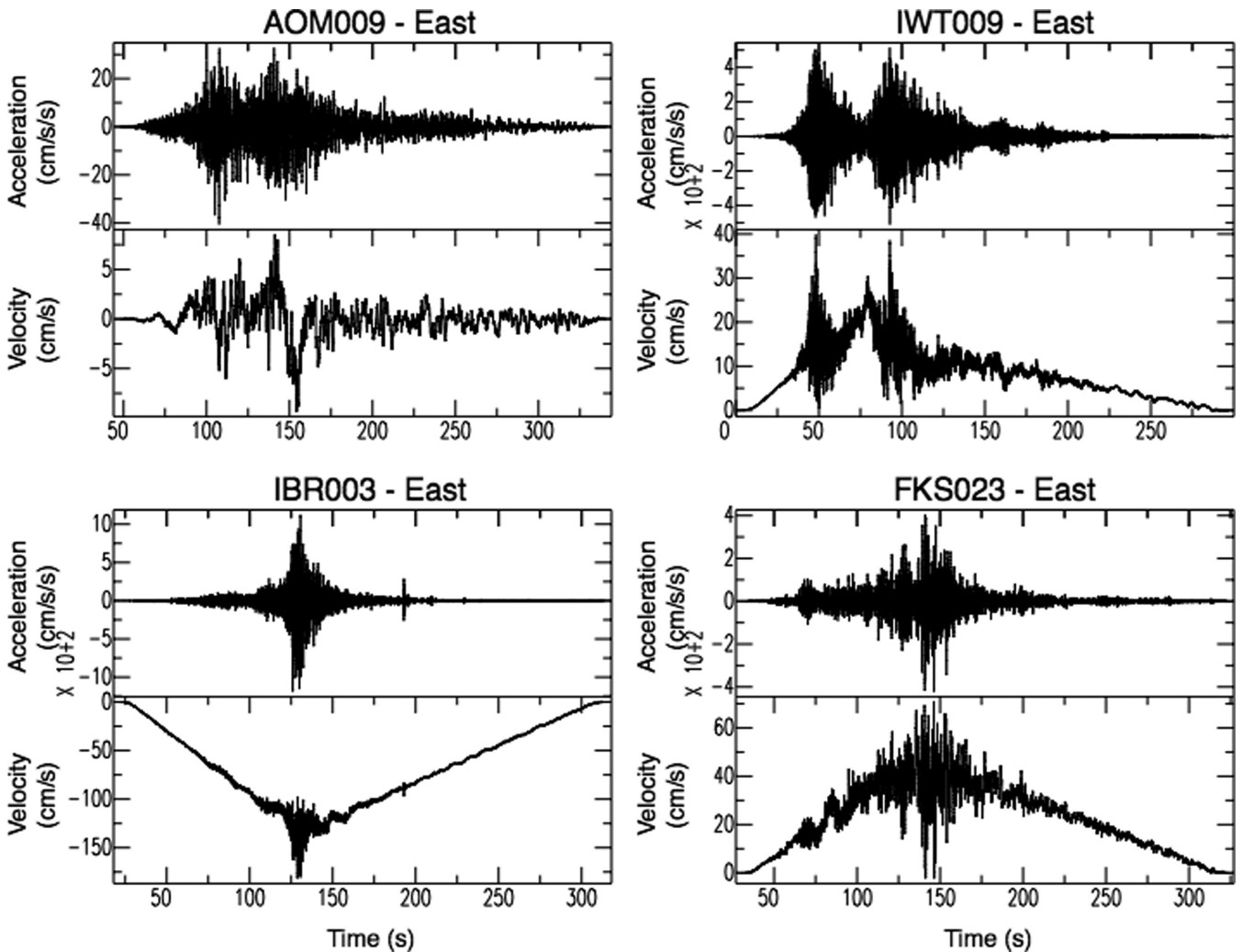


Figure 11. Non-linearity in the acceleration seismograms observed at some K-NET stations after integration. For each station, the top row shows the unprocessed strong-motion records and the bottom row shows the velocity seismogram obtained after integration of the acceleration seismogram. IWT009, IBR003 and FKS023 show evidence of instrument problems whereas AOM009 integrates correctly.

Table 2 shows that the source time function convolved with the GFs prior to any moment tensor calculations influences the output moment magnitude as well as the fit between the synthetics and the data. The moment magnitude is found to increase with increasing source duration. On the other hand, the origin time of the earthquake is found to decrease with increasing source duration. A source time function of 100 s was chosen in the analysis because it best recovers the data in the moment tensor inversion (Table 2). The source time duration of an earthquake could thus be derived from this analysis if multiple sets of elementary seismograms convolved with different source time functions were pre-processed and considered in parallelized source inversions. Also, we find that the variation in the rise time has very limited effects on the best location, and on the mechanism of the earthquake. This is encouraging for further studies and applications to other earthquakes in the area as well as in other regions where great earthquakes occurs. For comparison, Guilhem & Dreger (2011) used a source time function of 84 s for their analysis of synthetic M 8.2 to M 8.4 earthquakes off the coast of Mendocino in northern California.

The main advantage of using data from strong-motion stations is the capability of that instrumentation to record motions on scale ($\pm 4 \times g$) with a response in acceleration flat to DC. Modern strong motion instruments have very large dynamic range (>140 db) enabling robust recording of even very low frequency acceleration. We note however that there can be problems with these data. For example, when processing the data of the selected strong-motion stations of the K-NET network we found that several (IBR003, IWT009 and FKS023) lead to incorrect moment tensor inversions (Fig. 10). Inspection of the raw acceleration records did not reveal any obvious problems. However, after integration to velocity, the records displayed kinks on all three components (Fig. 11) suggesting that they suffered from loss of linearity due to a loss of phase-lock in the feedback mechanisms. Another possibility is that the accelerometers are sensitive to ground tilt. Ellsworth (personal communication,

2011) compared nearby continuous GPS records and found that at several sites the accelerometers appeared to suffer some bias due to ground tilt, especially on the horizontal components that are more sensitive to tilt. More analyses of the behaviour of strong-motion instruments driven by high levels of ground shaking and possible large amplitude tilts are necessary for a better understanding of their response to such motions, and how to better prepare site installations for long-period acceleration response.

Both clipping in raw weak motion data and data from continuous high rate GPS instruments could be used to verify whether an event is large and the strong motion data should be preferred in its analysis. Fig. 12 compares the theoretical velocity output of a radially oriented STS1 instrument in digital counts at station MYG015 for modelled reverse point-source earthquakes with magnitudes ranging between 6 and 9 located at the Tohoku-oki epicentre. The displacement for the M 9 earthquake is overestimated by the point source because the slip is forced to be concentrated at a single point. Nonetheless for the other magnitudes, the distance to the station does not preclude the point-source assumption. Fig. 12 shows that the digital signal clips between a M 6 and M 7 earthquake at 175 km distance. However, these two model events do not produce significant static offsets unlike the M 8 and M 9 seismic events (Fig. 12). Tracking the digital counts of the raw weak motion data and the static offset from continuous GPS data could help to better monitor the seismicity especially when the best solutions obtained by the short- and long-period scanning algorithms provide similar VRs. As a consequence they could be used to confirm whether a significant earthquake occurred. This emphasizes the need to continuously record strong-motion data. This is currently not done at the K-NET network, where data acquisition is event-triggered. Additionally, continuous high-rate GPS data could be used directly to estimate the long-period acceleration or velocity response, or used directly as displacement records in a implementation of this method (Melgar *et al.* 2011).

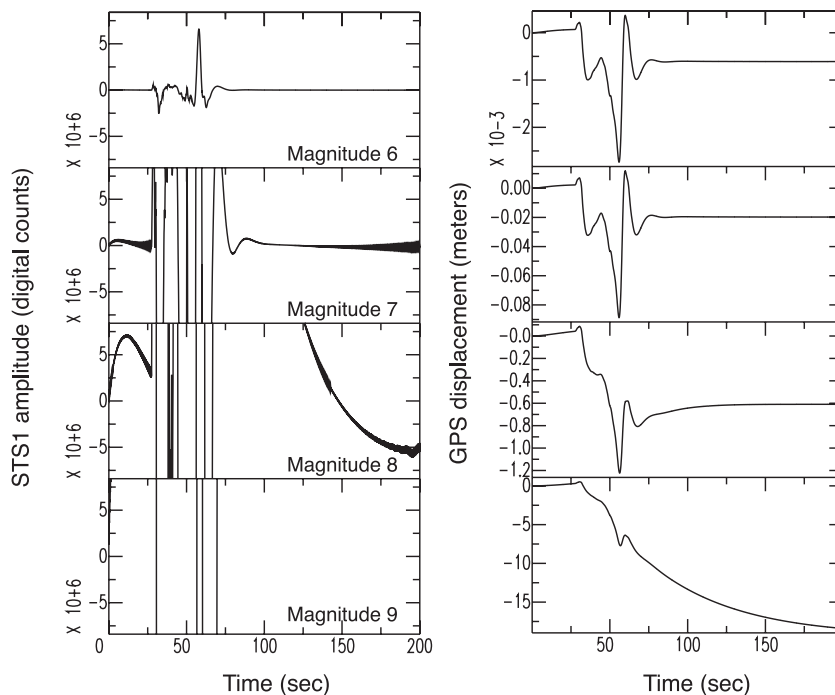


Figure 12. Comparison of the theoretical STS1 radial velocity component (amplitude in digital counts) for model reverse M 6 to M 9 earthquakes located at the M 9 Tohoku epicentre and recorded at 175 km at MYG015 station and the corresponding model displacement measured at the station in meters.

We show that the inversion of low-frequency, long-period (100–200 s) acceleration records at local to regional distance stations of the NIED K-NET could detect and locate the 2011 *M*9 Tohoku-oki earthquake, as well as recover unsaturated estimates of the seismic moment tensor. The analysis shows that robust results could be obtained within 8 min following the origin time of the main shock and therefore could be utilized for tsunami early warning if the method were included in the real-time processing scheme. Using very long-period waveforms (100–200 s) and an extended inversion window (8 min) we show that the system does not saturate for very large earthquakes, unlike classical techniques. Indeed we recover the moment magnitude and can recover the moment tensor of the event with a VR larger than 70 per cent. By limiting the inversions to be performed on sources located only on the slab itself and using QFS GFs to better image the extended rupture earthquake, we show that only 1/5 of the virtual source locations are needed and that detection, location and source parameter estimation are not adversely affected. This reduces the computational demands significantly. The time needed to perform the inversions depends however on the system used for the algorithm, the length of the inversions and the size of the studied region (i.e. number of point sources). Our algorithm ran on a 8-core sun computer, presently utilizing only 1 core. All elementary seismograms were pre-processed and entered in memory prior to any computation. Given these parameters the algorithm can process 5000 point sources for four three-component stations with a time step of 2 s. The total processing time for all of the virtual sources is less than the imposed 2 s time step. If parallelized or if fewer inversions are required, which is the case of when using QFS GFs, more station configurations, finite source lines, source durations, and/or multiple directivity cases could be tested simultaneously while trying to keep the time step of 2 s.

The proposed method has been shown to correctly characterize earthquakes in the near-field in northern California (Guilhem & Dreger 2011) and in Japan (Tsuruoka *et al.* 2009a), as well as for great earthquakes. To implement it in other regions the sensitivity of results to assumed velocity structures, optimal frequency passbands, and station availability need to be considered. This can be obtained thanks to extensive tests using multiple real and/or synthetic earthquakes located in the region of interest. In addition, the geometries of the extended source models (QFSGF) and of the station distribution have to be defined in advance. They need to be planned according to prior earthquake history in a given region, to potential zones where coupling has been determined, and/or to earthquake models expected to occur in a region of interest. Finally, the potential extension of the grid to the outer rise region should also be considered in this case intraplate events in regions with a history of outer rise activity, or simply to account for such a possibility as demonstrated by the 2012 April 11 *M*w 8.6 strike-slip earthquakes.

ACKNOWLEDGMENTS

Supported by the U.S. Geological Survey through external awards G10AP00069 and G12AP20007 and, by the Cooperative Institute for Alaska Research with funds from the National Oceanic and Atmospheric Administration under cooperative agreement NA08OAR4320751 with the University of Alaska. We thank EPSL editor Frank Krueger, reviewer Simone Cesca and an anonymous reviewer for their constructive advices. Strong motion data of the 2011 *M* 9 Tohoku-oki, Japan earthquake from the K-NET, National Research Institute for Earth Science and Disaster Prevention (NIED). Berkeley Seismological Laboratory contribution number 12–16.

REFERENCES

- Ammon, C.J., Lay, T., Kanamori, H. & Cleveland, M., 2011. A rupture model of the 2011 off the Pacific coast of Tohoku earthquake, *Earth Planets Space*, **63**, 693–696.
- Blewitt, G., Hammond, W.C., Kreemer, C., Plag, H.-P., Stein, S. & Okal, E., 2009. GPS for real-time source determination and tsunami warning systems, *J. Geod.*, **83**(3–4), 335–343.
- Brune, J.N., 1970. Tectonic stress and the spectra of seismic shear waves from earthquakes, *J. geophys. Res.*, **75**(26), 4997–5009.
- Clinton, J.F. & Heaton, T.H., 2002. The potential advantages of a strong-motion velocity meter over a strong-motion accelerometer, *Seismol. Res. Lett.*, **73**, pp. 332–342.
- Duputel, Z., Rivera, L., Kanamori, H., Hayes, G.P., Hirshorn, B. & Weinstein, S., 2011. Real-time W phase inversion during the 2011 off the Pacific coast of Tohoku Earthquake, *Earth Planets Space*, **63**(7), 535–539.
- Fukuyama, E. & Dreger, D., 2000. Performance test of an automated moment tensor determination system for the future “Tokai” earthquake, *Earth Planets Space*, **52**, 383–392.
- Guilhem & Dreger, 2011. Rapid detection and characterization of large earthquakes using quasi-finite-source Green’s functions in continuous moment tensor inversion, *Geophys. Res. Lett.*, **38**(L13318), doi:10.1029/2011GL047550.
- Hayes, G.P., Earle, P., Benz, H., Wald, D. & Briggs, R., the USGS/NEIC Earthquake Response Team, 2011. 88 hours: the US Geological Survey National Earthquake Information Center response to the March 11, 2011 *M*w 9.0 Tohoku earthquake, *Seismol. Res. Lett.*, **82**(4), 481–493.
- Hayes, G.P. & Wald, D.J., 2009. Developing framework to constrain the geometry of the seismic rupture plane of subduction interface a priori—a probabilistic approach, *Geophys. J. Int.*, **176**, 951–964.
- Hayashi, Y., Tsumahima, H., Hirata, K., Kimura, K. & Maeda, K., 2011. Tsunami source area of the 2011 off the Pacific coast of Tohoku earthquake determined from tsunami arrival times at offshore observation stations, *Earth Planets Space*, **63**, 809–813.
- Hirshorn, B. & Weinstein, S., 2009. Rapid estimates of earthquake source parameters for tsunami warning, in *Encyclopedia of Complexity and Systems Science*, pp. 10370, ed. Meyers, A., Springer, New York.
- Jost, M.L. & Hermann, R.B., 1989. A student’s guide to and review of moment tensors, *Seismol. Res. Lett.*, **60**, 37–57.
- Kanamori, H. & Rivera, L., 2008. Source inversion of W phase: speeding up seismic tsunami warning, *Geophys. J. Int.*, **175**, 222–238.
- Kawakatsu, H., 1998. On the realtime monitoring of the long-period seismic wavefield, *Bull. Earthq. Res. Inst.*, **73**, 267–274.
- Lay, T. *et al.*, 2005. The Great Sumatra-Andaman earthquake of 26 December 2004, *Science*, **308**, doi:10.1126/science.1112255.
- Lay, T., Yamazaki, Y., Ammon, C.J., Cheung, K.F. & Kanamori, H., 2011. The 2011 *M*w9.0 off the Pacific coast of Tohoku Earthquake: comparison of deep-water tsunami signals with finite-fault rupture model predictions, *Earth Planets Space*, **63**, 797–801.
- Lomax, A. & Michelini, A., 2009. Tsunami early warning using earthquake rupture duration, *Geophys. Res. Lett.*, **36**(L09306), doi:10.1029/2009GL037223.
- Melgar, D., Bock, Y. & Crowell, B.W., 2011. Real-time moment tensor inversion and centroid location for large events from local and regional displacement records, in *Proceedings of the American Geophysical Union, Fall Meeting 2011*, San Francisco, California, USA, Abstract #S51F-06.
- Mori, N., Takahashi, T., Yasuda, T. & Yanagisawa, H., 2011. Survey of the 2011 Tohoku earthquake tsunami inundation and run-up, *Geophys. Res. Lett.*, **38**(L00G14), doi:10.1029/2011GL049210.
- Okada, Y., 2011. Preliminary report of the 2011 off the Pacific coast of Tohoku Earthquake, NIED. Available at http://www.bosai.go.jp/e/pdf/Preliminary_report110328.pdf, (last accessed 12 November 2012).
- PTWC, 2011. Tsunami bulletin number 001, issued at 05:55 UTC March 2011.
- Saikia, C.K., 1994. Modified frequency-wavenumber algorithm for regional seismograms using Filon’s quadrature: Modelling of Lg waves in eastern North America, *Geophys. J. Int.*, **118**(1), 142–158.

- Shao, G., Li, X., Ji, C. & Maeda, T., 2011. Preliminary result of the March 11th, 2011 Mw9.1 Honshu earthquake. Available at: http://www.geol.ucsb.edu/faculty/ji/big_earthquakes/2011/03/0311_v3/Honshu.html10.1093/gji/ggs045.html, (last accessed 12 November 2012).
- Tsuruoka, H., Kawakatsu, H. & Urabe, T., 2009a. GRiD MT (grid-based real-time determination of moment tensors) monitoring the long-period seismic wavefield, *Phys. Earth planet. Inter.*, **175**, 8–16.
- Tsuruoka, H., Rivera, L., Kawakatsu, H. & Kanamori, H., 2009b. Realtime source inversion using W-phase and GRiD MT for regional tsunami early warning, AGU 2009, S13A-1732.
- Vigny, C. *et al.*, 2011. The 2010 Mw8.8 Maule megathrust earthquake of central Chile monitored by GPS, *Science*, **332**(6036), 1417–1421.
- Wang, C.Y. & Herrmann, R.B., 1980. A numerical study of P-, SV-, and SH-wave generation in a plane layered medium, *Bull. seism. Soc. Am.*, **70**, 1015–1036.
- Yamazaki, Y. & Cheung, K.F., 2011. Shelf resonance and impact of near-field tsunami generated by the 2010 Chile earthquake, *Geophys. Res. Lett.*, **38**(L12605), doi:10.1029/2011GL047508.
- Yue, H. & Lay, T., 2011. Inversion of high-rate (1sps) GPS data for rupture process of the 11 March 2011 Tohoku earthquake (Mw9.1), *Geophys. Res. Lett.*, **38**(L00G09).